CrossMark

Eolian sand sheet deposition in the San Luis paleodune field, western Argentina as an indicator of a semi-arid environment through the Holocene

Steven L. Forman [a], Alfonsina Tripaldi [b], Patricia L. Ciccioli [b,*]

[a] Dept. of Geology, One Bear Place #97354, Baylor University, Waco, TX 76798-7354, United States
[b] IGEBA-CONICET, Dept. of Geological Sciences, University of Buenos Aires, Ciudad Universitaria, Buenos Aires C1428EHA, Argentina

ABSTRACT

Eolian deposits are common in the western Pampas of Argentina, and most are assumed to be associated with glacial conditions. Stratigraphic and sedimentologic studies coupled with OSL dating in San Luis Province document for the first time a nearly continuous sequence of eolian sand sheet deposits that span most of the Holocene. Petrology and geochemical analyses indicate that the source of the sand is from pre-existing Pleistocene eolian sediments. Sand sheet deposition between ca. 12 and 1 ka is associated with sparse, Monte-type vegetation that occurs with drier conditions (MAP 450–100 mm) than the late 20th century (~700 mm). This paleoenvironmental inference is consistent with nearby pollen and lake level records. A persistent semi-arid environment in western Argentina during the Holocene may reflect sustained warm SSTs in the western equatorial Atlantic Ocean, which may have suppressed the pressure gradient between the South Atlantic Anticyclone and Chaco Low and thus, the flux of summer moisture to western Argentina. There appears to be a paleoclimatic "dipole" response between a dry western Argentina and a wet southeastern Brazil, which is consistent with the increasing strength of the South American Monsoon through the Holocene. Sand sheet accretion appears to cease by 800 to 200 years ago with wetter conditions and succession to Espinal vegetation prior to European contact.

© 2014 Elsevier B.V. All rights reserved.

1. Introduction

Presently stabilized and active dune fields are common across the Argentinian Pampas to the Andean Piedmont (e.g. Iriondo and Kröhling, 1995; Tripaldi and Forman, 2007; Zárate and Tripaldi, 2012). These eolian systems with associated loess deposition were active during the last glacial cycle and potentially prior glaciations (Zárate, 2003 and references therein). However, recent studies have documented that many eolian systems in western Argentina were active in the Holocene (Tripaldi and Forman, 2007; Zárate and Tripaldi, 2012; Mehl et al., 2012) and possibly concomitant with loess deposition in the Pampas (Zárate, 2003; Kemp et al., 2006). Pollen records from across Argentina indicate broadly drying with the eastward expansion of Monte-type vegetation in the early and middle Holocene (Mancini et al., 2005), indicative of semi-arid conditions (<450 mm precipitation). In contrast to extreme and episodic wet conditions during the last glacial maximum (ca. 24 to 12 ka), pervasive drying is also documented in lacustrine sedimentary and other proxy records ca. 9 to 3 ka from the Bolivian and Chilean Altiplano and northwest Argentina (Markgraf, 1989; Villagrán and Varela, 1990; Sandweiss et al., 1999; Jenny et al., 2002; Abbott et al., 2003; Zech et al., 2009; Placzek et al., 2009; Blard et al., 2011; Tchilinguirian and Morales, 2013). Eolian deposition in the early and the middle Holocene is reported for the tropical Chaco Plain proximal to rivers, between ~18 and 21°S east of the Andes, and is interpreted to reflect increased aridity (Latrubesse et al., 2012), though this record may also reflect an increase in sediment supply. In western Argentina drying may have been severe enough to restrict human habitation in southern Mendoza Province (Fig. 1), as evidenced by the disappearance of archeological sites between ca. 6 and 4 ka (Gil et al., 2005; Zárate et al., 2005).

There is a noticeable precipitation gradient from east to west across the Pampas to the foothills of the Andes (cf. Garreaud et al., 2009). The eastern Pampas has a mean annual precipitation >1000 mm, whereas <300 mm of precipitation is delivered annually to the Andean Piedmont (Cabido et al., 2008). Well-documented ecological regions are present from east to west including the Pampean Grassland, the Espinal and the Monte phytogeographic provinces (cf. Cabrera, 1976), which parallel this precipitation gradient (Labraga and Villalba, 2009). The Espinal (~450–600 mm MAP) is savannah-like with grasses and scattered trees, whereas the drier Monte (~100–450 mm MAP) is a shrub steppe
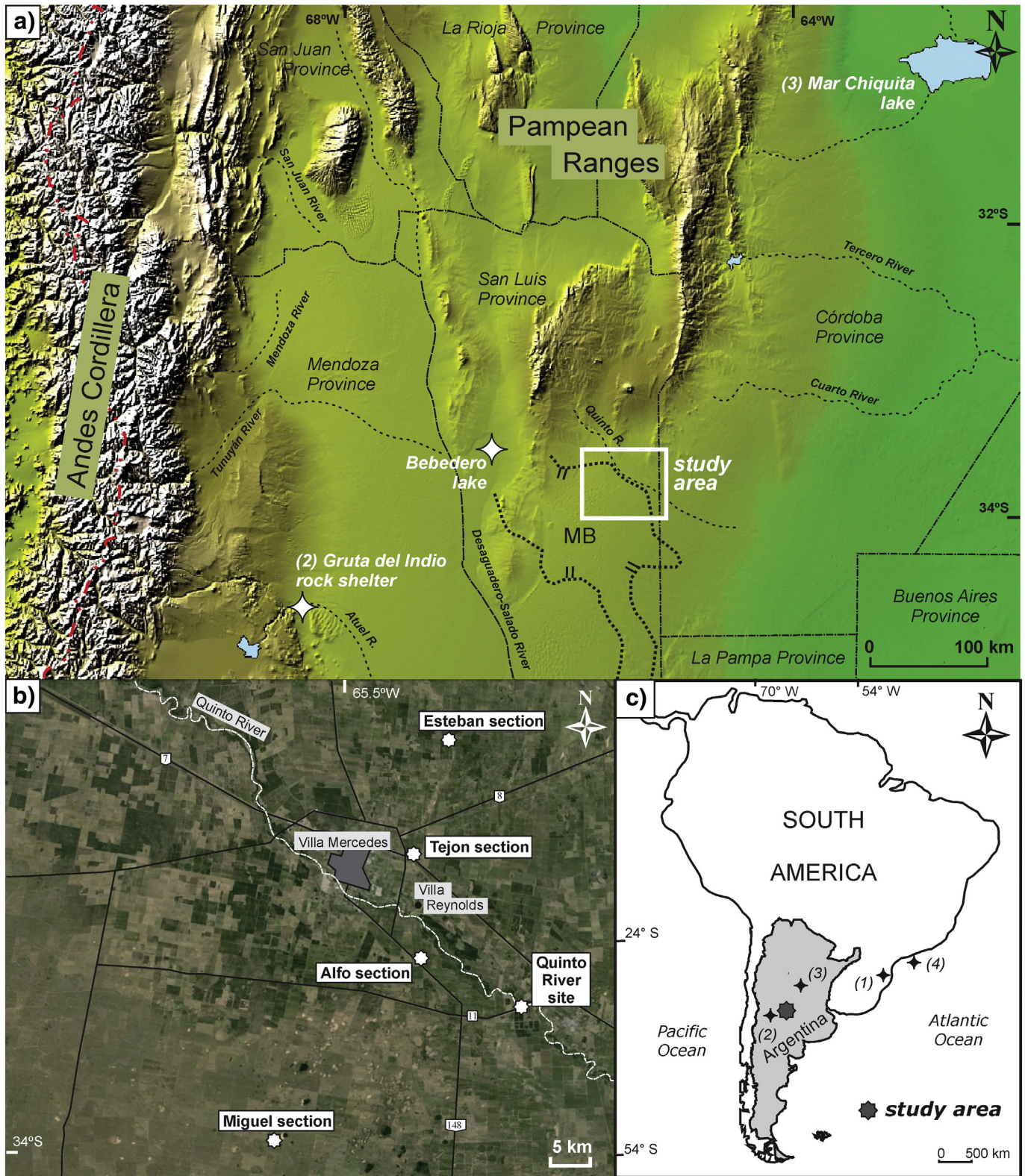
Fig. 1. Location maps, (a) SRTM3 digital elevation data of the study area in western Pampas (San Luis Province, Argentina), mentioned localities and outlined Mercedes Basin (MB, after Kostadinoff and Gregori, 2004); (b) study sites from the San Luis paleodune field; (c) analyzed South American localities with Holocene record: (1) Botuverá cave (Brazil; Wang et al., 2006), (2) Gruta del Indio rock shelter (Argentina; D'Antoni, 1983; Markgraf, 1983), (3) Mar Chiquita lake (Argentina; Piovano et al., 2009), (4) marine core derived SSTs (Brazilian platform; Pivel et al., 2013).

with scattered *Prosopis* sp. woodlands, often where groundwater is accessible (Paruelo et al., 2007). A majority of precipitation (>70%) is delivered to western Argentina during the austral spring and summer (October to March) (Silva and Kousky, 2012). Mean maximum summer

temperatures during this rainy season can often exceed 35 °C, enhancing evaporative losses.

The source of this precipitation and warmth for western Argentina is the pressure gradient between a thermal-orographic dynamic Chaco

Low located east of the Andes and the subtropical South Atlantic Anticyclone (Compagnucci et al., 2002; Doyle and Barros, 2002; Barros et al., 2008). This pressure gradient increases during the austral summer with a maximum in solar insolation, resulting in northeasterly flow and the net import of moisture from the Atlantic Ocean. Another important source of moisture is the low-level meridional Chaco Jet which brings warm and moist air derived from tropical jungles and humid lowlands of Bolivia and Brazil southward along the eastern margin of the Andes (Wang and Paegle, 1996; Salio et al., 2002; Marengo et al., 2004). The subtropical Andes Mountains with a mean peak elevation of 4000 m are an effective barrier for the direct import of moisture from the Pacific Ocean, though middle tropospheric Rossby Wave trains in the subtropics and extratropics associated with strong El Niño events may enhance precipitation in western Argentina with advected sources from the Atlantic Ocean and the western Amazon Basin (Grimm, 2003; Andreoli and Kayano, 2004; Barros et al., 2008; Mendes da Silva and Ambrizzi, 2010).

In the past century there has been considerable variability in precipitation in western Argentina and with a resultant landscape scale response. In the 1930s there was a severe drought associated with a 30 to 66% deficit in precipitation that was concomitant with agriculture-related landscape disturbance, which resulted in pervasive reactivation of dune systems (Compagnucci et al., 2002; Tripaldi et al., 2013). In contrast, since the 1960s the western Pampas has been inordinately wet; a result of a 20 to 30% increase in precipitation (Pasquini et al., 2006; Agosta and Compagnucci, 2008). New rivers and lakes have formed over the past decade reflecting both increase in precipitation, and also a decrease in evapotranspiration with further expansion of agriculture (Viglizzo et al., 2010; Contreras et al., 2013). The climatology is not fully resolved for these extreme states in precipitation, particularly beyond annual timescales (cf. Seager et al., 2010). Doyle and Barros (2002) observed that wet conditions in western Argentina during the late 20th century are associated with a strengthened South Atlantic Convergent Zone (SACZ) and an increase in meridional transport of moisture from the South American and the Chaco Low Level jets. Also, cooler sea surface temperatures (SSTs) in the equatorial South Atlantic Ocean tend to strengthen the South Atlantic Anticyclone and the summer-time pressure gradient with the Chaco Low, increasing the landward flux of Atlantic-derived moisture (Fig. 2). Dry conditions are synoptically less well resolved, but appear to be associated with a weakened SACZ and a more zonal transport of moisture by the South American Low Level Jet toward southeastern Brazil (Liebmann et al., 2004). Warmer equatorial SSTs tend to weaken the South Atlantic Anticyclone and associate moisture flux from the Atlantic Ocean into western Argentina, whereas wet conditions prevail in coastal southeastern Brazil (Doyle and Barros, 2002) (Fig. 2). Numerical climate modeling indicates that warmer tropical Atlantic SST anomalies in the 1930s contributed to drought conditions in western Argentina (Seager et al., 2010). This synoptic analysis indicates that there may be a climatic "dipole" with a synchronous wet southeastern Brazil and dry western Argentina (cf. Cruz et al., 2009; Morrill et al., 2013).

There is limited knowledge of Holocene paleoenvironments and moisture variability in west-central Argentina (cf. Labraga and Villalba, 2009). A pollen record from the rock shelter Gruta del Indio on the Andean piedmont (site 2, Fig. 1a,c) indicates a transition from cool and wet Patagonia-dominated species to drier Monte-dominated species ~14 to 11.5 ka (D'Antoni, 1983), which persisted until ~5.2 ka and is associated with an increase in mean temperature and diminished summer precipitation (Markgraf, 1983). Records from Salinas del Bebedero, located ~100 km west of the Sand Luis paleodune field (Fig. 1), reflect mostly subaerial conditions between ~12 and 11 ka, based on the lack of diatom frustules and abundance of archeological material (González and Maidana, 1998). The sedimentology and $\delta^{13}C$ on bulk organic matter from a core from Mar Chiquita Lake (site 3, Fig. 1a,c) indicate fluctuating and mostly low lake levels during the Holocene, with particularly dry periods at ca. 8.2 and 3.4 ka (Piovano et al., 2004, 2009).

An important record in the southern subtropics is an oxygen isotope time series for speleothems from Botuverá Cave in southeastern Brazil (site 1 in Fig. 1c), that indicates increasing monsoonal precipitation through the Holocene (Cruz et al., 2005; Wang et al., 2006). In turn, sediment records from the western South Atlantic Ocean (site 4 in Fig. 1c) indicate warming of SSTs post 13 ka, noticeable cooling from ca. 10 to 8.1 ka and sustained warmth for much of the last ca. 8 ka (Toledo et al., 2007; Pivel et al., 2013), consistent with broadly wetter conditions in southern Brazil through the Holocene.
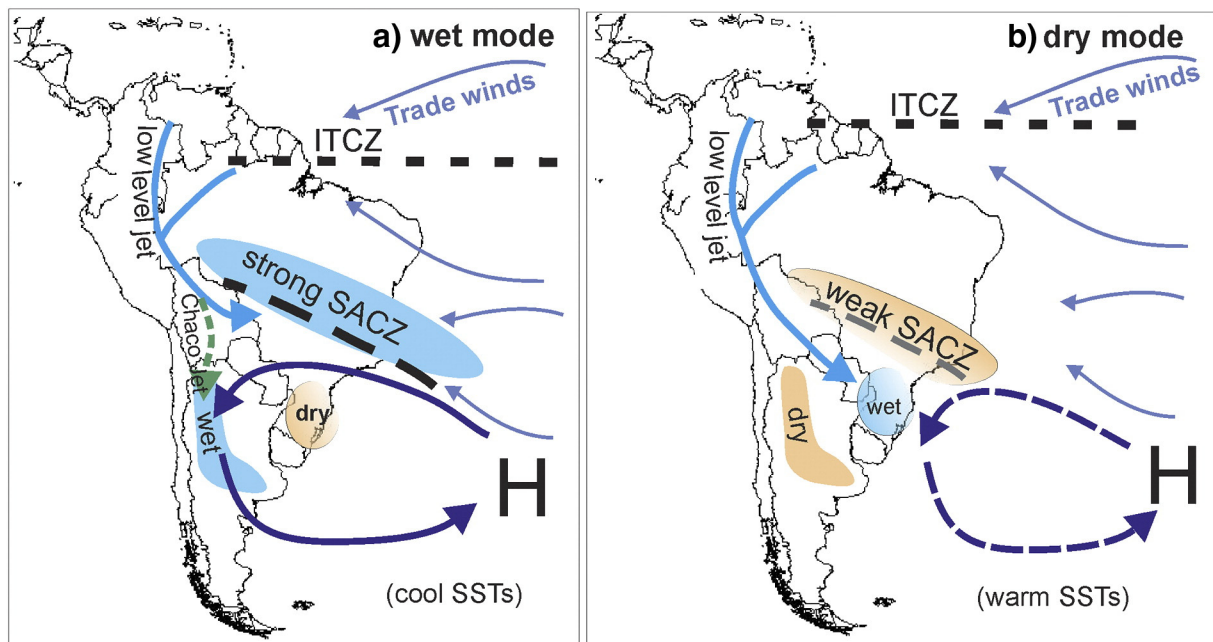

Fig. 2. Depiction of low level circulation for two climatic extremes, associated with wet (a) and dry (b) conditions in western Argentina. Abbreviations: ITCZ, Intertropical Convergence Zone; SACZ, South Atlantic Convergence Zone, SST, sea surface temperature.
Modified from Barros et al. (2002).

We hypothesize that if a climatic dipole existed in the Holocene, similar to that of the 20th century (Doyle and Barros, 2002; Cruz et al., 2009), a dry western Pampas should be broadly concurrent with wet conditions in southeastern Brazil and drier climate in northeastern Brazil. To test this hypothesis, we studied a previously documented eolian-sand depositional record in San Luis Province, western Argentina, that spans the Holocene (Tripaldi and Forman, 2007) and is currently a mesic environment with an Espinal savannah (Paruelo et al., 2007). Geomorphic and stratigraphic observations are presented in different contexts in the Mercedes depositional basin, indicating a sedimentologic response to widespread drying. Chronologic control is provided by optically stimulated luminescence dating of small aliquots of quartz grains and this approach has yielded previously a stratigraphically consistent chronology (Tripaldi and Forman, 2007; Tripaldi et al., 2013). Granulometry, petrography and geochemistry of eolian sands provide new insights on depositional processes and provenance of sand during the Holocene (cf. Tripaldi et al., 2010). This study documents pervasive sand sheet deposition about simultaneous to the Younger Dryas chronozone and nearly continuous eolian sand deposition for much of the Holocene with an inferred persistence of a semi-arid environment.

2. Geomorphic context

The San Luis paleodune field is part of an inferred larger late Quaternary eolian system called the "Pampean Sand Sea" (e.g. Iriondo and Kröhling, 1995; Iriondo, 1999) that covers most of central Argentina. The San Luis paleodune field is a mesic environment with ~730 mm of annual precipitation (AD 1980–2000) and a mean and maximum temperature of 17 °C and 24 °C, respectively. This landscape is highly cultivated, but in areas supports a savannah-type vegetation with surface soils with well developed and organic-rich A horizons. Seasonal wind data from Tripaldi and Forman (2007), presented as wind drift potentials, indicate persistent winds from the northeast and more northerly components in the winter and the fall.

This paleodune field is characterized by a stacked sequence of eolian sands that show different degrees of deflation and eolian reworking by blowout and parabolic dunes (Tripaldi and Forman, 2007). Historical accounts, photographs and stratigraphic studies indicate that these landforms formed in the 20th century, many during a dry period coupled with anthropogenic disturbance in the 1930s (Tripaldi et al., 2013). These young blowout dunes, with inferred paleowind direction from the northeast, are superimposed on and composed of rework sand from presently vegetated, larger lobate parabolic dunes and intervening sand sheet deposits.

3. Methods

3.1. Stratigraphy and sedimentology

We present stratigraphic, sedimentologic, and pedologic observations for seven sections at four sites in the San Luis paleodune field (cf. Tripaldi and Forman, 2007; Zárate and Tripaldi, 2012). These sequences are characterized by depositional units of eolian sand with a paleosol at or near the section base. At one site, near the section top, is the Quizapú Ash from the 1932 eruption of Descabezado-Cerro Azul volcano in Chile (Hildreth and Drake, 1992). Usually, eolian stratigraphic successions contain a fragmentary record of depositional periods and associated hiatuses because of the unknown completeness associated with erosion and pedogenesis (e.g. Tripaldi and Forman, 2007; Singhvi and Porat, 2008). Thus, we studied multiple sections in this stabilized dune field located in different depositional and geomorphic contexts, which collectively may reflect a more complete history of eolian deposition, landscape stability, and inferred paleoenvironmental changes. At many localities tens to hundreds of meters of these sections are laterally exposed allowing us to evaluate the continuity of stratigraphic units. Sections were studied with attention to sedimentologic and pedogenic details. The attitude of beds was recorded to assess paleowind directions. These measurements are most meaningful where bed dips are >5°. Also, we recorded variability in bed thickness, nature of bed contacts and the associated granulometry. Attention was focused carefully on bedding planes and unit contacts to assess if there were hiatuses in deposition, sometimes indicated by the presence of a buried soil or localized bioturbation. The recognition and lateral tracing of a buried soil is pivotal because this stratigraphic marker reflects landscape stability, possibly associated with relatively mesic conditions. We used well vetted soil stratigraphic and geomorphic approaches (Birkeland, 1999; Tripaldi and Forman, 2007). All soil colors are assessed in the dry state. Buried soils show clear signs of rubification and secondary accumulation of clay and silt and in places there is evidence for precipitation of pedogenic carbonate. Eolian stratigraphic units representing discrete depositional events were defined by either bounding buried soils or sedimentologic characteristics.

3.2. Sediment granulometry and composition

The granulometry was determined for a majority of stratigraphic units with samples often retrieved at the same level of samples for OSL dating. Particle size analysis provides valuable complementary information to infer depositional processes, render paleoenvironmental interpretations and evaluate pedogenic alterations. Granulometry was determined using a Malvern 2000 laser-based Mastersizer at the INCITAP-CONICET, Universidad Nacional de La Pampa (Argentina). Prior to analysis sediments were soaked in H_2O_2 and HCl to eliminate possible cementing substances such as organic matter and $CaCO_3$ and dispersed into an ultrasonic bath. The sand, silt and clay percentage (Folk et al., 1970) was determined for each deposit along with associated statistical parameters (graphic formulas after Folk and Ward, 1957; Appendix 1). Data was analyzed through histograms and cumulative probability frequency curves and the basic granulometry is plotted with sections (Fig. 6) to evaluate variability stratigraphically.

The petrographic and geochemical compositions of sand samples were determined to evaluate the potential source of sediments. Key provenance indicators are the presence and proportion of different types of feldspars; volcanic, sedimentary and metamorphic rock fragments, and glass particles (e.g. Kasper-Zubillaga and Dickinson, 2001; Tripaldi et al., 2010). The composition of sand may be independent of the source rocks reflecting the physiography and the chemical weathering in the source area of the sediment (cf. Basu, 1985). However, the studied Holocene sediments showed little evidence of chemical weathering, and paleosol levels were avoided, thus the petrographic composition is analyzed to infer sediment source of the dune fields.

The petrographic analysis was accomplished by grain counting of thin sections of medium to fine sand fractions mounted in epoxy resin (Potter et al., 2001; Garzanti et al., 2005). In each sample, 300 grains were counted by the Gazzi–Dickinson method (Gazzi, 1966; Dickinson, 1970). Roundness was estimated by visual comparison in thin sections after Powers (1953). The recognized petrographic components in the eolian sand are listed in the Appendix 2. Quartz (Q) grains were separated in monocrystalline (Qm) and polycrystalline (Qp) types, whereas among feldspar (F), K-feldspar (FK), plagioclase (P) and microcline (M) were recognized. Rock fragments (L) include volcanic (Lv), metamorphic (Lm) and sedimentary (Ls) lithics. Volcanic sand grains (LvT) were subdivided into felsic (Lvf), microlithic (Lvm) and lathwork (Lvl) textures, corresponding to acid, intermediate and basic magma composition, respectively. Fresh glass shards and pumices (Glass) were also recognized. Metamorphic fragments (Lm) include phyllite, schist and amphibolite types, and Lp consists of those lithics with plutonic textures. Sedimentary rock fragments (LsT) comprise siliciclastic (Lss) and carbonate (Lsc) lithic fragments. Accessory minerals (acc) include biotite, muscovite, amphibole, pyroxene, zircon and the opaque fraction. Sands are classified according to the Q:F:L (quartz, feldspars and rock fragments) ratio following Folk et al. (1970).

Concentrations of SiO_2, Al_2O_3, Fe_2O_3 (total), MnO, MgO, CaO, Na_2O, K_2O, TiO_2, P_2O_5, Ba, Sr, Zr, Y, Sc, Be, V, Th, and U were determined on total sediment aliquots by inductively coupled plasma mass spectrometry by Activation Laboratory LTD, Ontario, Canada (Appendix 3). The elemental analysis is used to evaluate the presence of distinct geochemical signatures in the eolian deposits (e.g. Pease and Tchakerian, 2003; Tripaldi et al., 2010).

3.3. Optically stimulated luminescence dating

The eolian strata were sampled for luminescence dating only after there was a full understanding of sedimentology, stratigraphy, extent of soil development, and the associated lateral changes in buried soils and eolian units. We extracted at least two samples from luminescence dating from each eolian stratigraphic unit. We favored sampling primary eolian depositional strata and avoided horizons exhibiting signs of pedogenesis. Sediments were often sampled at or near stratigraphic unit contacts to address the timing and duration deposition. Also at the Miguel and the Quinto River overlook sections nine OSL samples were collected at approximately 25 to 30 cm intervals from about 4-m-thick sequences of strata of bedded sand sheet from which five and six samples respectively were dated. At the Miguel section the chosen samples for dating were from bedded intervals, avoiding massive bioturbated intervals. In contrast, samples for OSL dating at the Quinto River overlook site were from intervals between 80 and 50 cm. The dated samples provide insights into internal age structure for this pervasive sand sheet deposit. Samples were taken using light tight 5 cm diameter and 15 cm long sections of black ABS pipe, which were hammered gently into the sediment face at the desired sampling level.

Single aliquot regeneration (SAR) protocols (Murray and Wintle, 2003; Wintle and Murray, 2006) were used in this study to estimate the apparent equivalent dose of the 63–100, 100–150 or 150–250 μm quartz fraction for 25 to 37 separate aliquots (Table 1). Each aliquot contained approximately 100 to 500 quartz grains corresponding to a 1 to 2 millimeter circular diameter of grains adhered (with silicone) to a 1 cm diameter circular aluminum disk. This aliquot size was chosen to maximize light output for the natural with excitation; smaller aliquots often yielded insufficient emissions (<400 photon counts/s). The sands analyzed have a SiO_2 content of 65% to 70% (Appendix 3) of the non-carbonate fraction and are predominantly moderately to poorly sorted with 10 to 26% quartz grains. The quartz fraction was isolated by density separations using the heavy liquid Na-polytungstate, and a 40-minute immersion in HF (40%) was applied to etch the outer ~10 μm of grains, which is affected by alpha radiation (Mejdahl and Christiansen, 1994). Quartz grains were rinsed finally in HCl (10%) to remove any insoluble fluorides. The purity of quartz separate was evaluated by petrographic inspection and point counting of a representative aliquot. Samples that showed >1% of non-quartz minerals were retreated with HF and rechecked petrographically. The purity of quartz separates was tested by exposing aliquots to infrared excitation (1.08 W from a laser diode at 845 ± 4 nm), which preferentially excites feldspar minerals. Samples measured showed weak emissions (<200 counts/s), at or close to background counts with infrared excitation, and ratio of emissions from blue to infrared excitation of >20, indicating a spectrally pure quartz extract (Duller, 2003).

An Automated Risø TL/OSL-DA-15 system (Bøtter-Jensen et al., 2000) was used for SAR analyses. Blue light excitation (470 ± 20 nm) was from an array of 30 light-emitting diodes that deliver ~15 mW/cm² to the sample position at 90% power. Optical stimulation for all samples was completed at an elevated temperature (125 °C) using a heating rate of 5 °C/s. All SAR emissions were integrated over the first 0.8 s of stimulation out of 40 s of measurement, with background based on emissions for the last 30- to 40-second interval. The luminescence emission for all quartz sands showed a dominance of a fast component (see Murray and Wintle, 2003) with >90% diminution of luminescence after 4 s of excitation with blue light (Fig. 3).

A series of experiments was performed to evaluate the effect of preheating at 180, 200, 220, 240 and 260 °C on isolating the most robust time-sensitive emissions and thermal transfer of the regenerative signal prior to the application of SAR dating protocols (see Murray and Wintle, 2003). These experiments entailed giving a known dose (20 Gy) and evaluating which preheat resulted in recovery of this dose. There was concordance with the known dose (20 Gy) for preheat temperatures above 200 °C with an initial preheat temperature used of 220 °C for 10 s in the SAR protocols. A "cut heat" at 160 °C for 10 s was applied prior to the measurement of the test dose and a final heating at 260 °C for 40 s was applied to minimize carryover of luminescence to the succession of regenerative doses. A test for dose reproducibility was also performed following procedures of Murray and Wintle (2003) with the initial and final regenerative dose of 9.8 Gy yielding concordant luminescence responses (at one-sigma error) (Fig. 3).

Calculation of equivalent dose by the single aliquot protocols was accomplished for 25 to 37 aliquots (Table 1). For all samples 83 to 100% aliquots were used for the final (D_e) distribution and age determination; only 55 aliquots (out of 880) were removed from the analysis because the recycling ratio was not between 0.90 and 1.10, the zero dose was >5% of the natural emissions or the error in equivalent dose determination is >10%. Equivalent dose (D_e) distributions, except for the youngest samples UIC2801 and UIC2805, were log normal and exhibited overdispersion values ≤20% (at two-sigma errors) (Table 1). An overdispersion percentage of a D_e distribution is an estimate of the relative standard deviation from a central D_e value in context of a statistical estimate of errors (Galbraith et al., 1999; Galbraith and Roberts, 2012). A zero overdispersion percentage indicates high internal consistency in D_e values with 95% of the D_e values within 2σ errors. Overdispersion values ≤20% are routinely assessed for small aliquots of quartz grains that are well solar reset, like eolian sands (e.g., Olley et al., 1998; Wright et al., 2011; Meier et al., 2013) and this value is considered a threshold metric for the calculation of a D_e value using the central age model of Galbraith et al. (1999). Overdispersion values >20% (at two sigma limits) indicate mixing or grains of various ages or partial solar resetting of grains; the minimum age model (three parameters) may be an appropriate statistical treatment for such data (Galbraith et al., 1999), and this model was used for quartz extracts for UIC2801 and UIC2805. The age of 70 ± 10 yr for sample UIC2805 is consistent with the age for a historic ash deposit of AD 1932 (Hildreth and Drake, 1992) immediately overlying this sample.

A determination of the environmental dose rate is needed to render an optical age, which is an estimate of the exposure of quartz grains to ionizing radiation from U and Th decay series, ^{40}K, and cosmic sources during the burial period (Table 1). The U and Th content of the sediments, assuming secular equilibrium in the decay series and ^{40}K, was determined by inductively coupled plasma-mass spectrometry (ICP-MS) analyzed by Activation Laboratory LTD, Ontario, Canada. The beta and gamma doses were adjusted according to grain diameter to compensate for mass attenuation (Fain et al., 1999). A significant cosmic ray component between 0.10 and 0.21 mGy/yr was included in the estimated dose rate taking into account the current depth of burial (Prescott and Hutton, 1994). A moisture content (by weight) of 5 ± 2%, or 10 ± 3%, was used in dose rate calculations, which reflects the variability in current field moisture conditions and the associated errors are consistent with the probable variability in water content during the burial period. The datum year for all OSL ages is AD 2000 to be compatible with previous reported ages in Tripaldi and Forman (2007) and Tripaldi et al. (2013).

4. Results

4.1. Section location in context to depositional basin and geomorphology

Seven measured sections of the Holocene eolian stratigraphic record are presented, with the following names: Quinto River overlook, Road

Table 1
Optically stimulated luminescence (OSL) data and ages on quartz grains from eolian deposits San Luis dune field, western Pampas, Argentina.

Sample	Laboratory number	Aliquots	Grain size (μm)	Equivalent dose (Gray)[a]	Over-dispersion (%)[b]	U (ppm)[c]	Th (ppm)[c]	K (%)[c]	H₂0 (%)	Cosmic dose (mGray/yr)[d]	Dose rate (mGray/yr)	OSL age (yr)[f]
SL08-04	UIC2371	30/30	63-100	14.46 ± 0.63	16 ± 2	2.4 ± 0.1	8.8 ± 0.1	2.22 ± 0.02	5 ± 2	0.18 ± 0.02	3.48 ± 0.23	4135 ± 300
SL08-06	UIC2372	30/30	63-100	15.49 ± 0.71	18 ± 2	2.4 ± 0.1	8.8 ± 0.1	2.19 ± 0.02	5 ± 2	0.17 ± 0.02	3.45 ± 0.22	4480 ± 330
SL08-08	UIC2373	30/30	63-100	21.24 ± 1.04	19 ± 2	2.5 ± 0.1	9.3 ± 0.1	2.21 ± 0.02	10 ± 3	0.16 ± 0.02	3.33 ± 0.21	6365 ± 505
SL08-11	UIC2375	30/30	63-100	16.27 ± 0.81	19 ± 2	2.3 ± 0.1	8.2 ± 0.1	2.10 ± 0.02	5 ± 2	0.18 ± 0.02	3.31 ± 0.22	4910 ± 380
SL08-13	UIC2499	33/35	63-100	38.12 ± 1.86	20 ± 3	3.0 ± 0.1	9.8 ± 0.1	2.12 ± 0.02	10 ± 3	0.16 ± 0.02	3.39 ± 0.22	11,210 ± 870
SL08-19	UIC2501	33/35	63-100	4.01 ± 0.15	22 ± 3	2.6 ± 0.1	9.0 ± 0.1	2.33 ± 0.02	2 ± 1	0.17 ± 0.02	3.77 ± 0.26	1070 ± 70
SL08-20	UIC2729	26/30	100-150	8.46 ± 0.23	20 ± 3	2.5 ± 0.1	8.9 ± 0.1	2.19 ± 0.02	5 ± 2	0.16 ± 0.02	3.35 ± 0.22	2515 ± 150
SL08-21	UIC2578	29/30	63-100	17.45 ± 0.78	17 ± 2	2.5 ± 0.1	8.8 ± 0.1	2.26 ± 0.02	5 ± 2	0.14 ± 0.01	3.51 ± 0.23	4960 ± 385
SL08-22	UIC2730	28/30	100-150	21.02 ± 1.06	19 ± 2	2.6 ± 0.1	9.1 ± 0.1	2.22 ± 0.03	5 ± 2	0.13 ± 0.01	3.39 ± 0.22	6185 ± 475
SL08-24	UIC2577	30/30	100-150	25.49 ± 1.10	14 ± 1	2.1 ± 0.1	7.5 ± 0.1	2.06 ± 0.02	5 ± 2	0.11 ± 0.01	3.00 ± 0.16	8490 ± 620
SL08-27	UIC2502	32/35	63-100	41.15 ± 1.98	16 ± 2	2.8 ± 0.1	9.3 ± 0.1	2.03 ± 0.02	10 ± 3	0.09 ± 0.01	3.36 ± 0.22	12,260 ± 910
SL08-35	UIC2344	28/30	63-100	5.61 ± 0.31	23 ± 3	1.9 ± 0.1	6.7 ± 0.1	2.15 ± 0.02	2 ± 1	0.21 ± 0.02	3.24 ± 0.21	1720 ± 140
SL08-36	UIC2731	30/30	100-150	25.49 ± 1.10	12 ± 2	2.1 ± 0.1	7.5 ± 0.1	2.06 ± 0.02	5 ± 2	0.11 ± 0.01	3.00 ± 0.16	8490 ± 620
SL08-37	UIC2346	29/30	63-100	33.78 ± 1.72	20 ± 3	2.0 ± 0.1	7.3 ± 0.1	2.09 ± 0.02	10 ± 3	0.14 ± 0.01	2.95 ± 0.15	11,455 ± 940
SL08-39	UIC2345	30/30	63-100	63.58 ± 2.66	12 ± 2	2.3 ± 0.1	10.1 ± 0.1	2.23 ± 0.02	5 ± 2	0.11 ± 0.01	3.51 ± 0.23	18,130 ± 1300
SL10-01	UIC3278	27/30	100-150	15.99 ± 0.84	21 ± 3	2.1 ± 0.1	7.2 ± 0.1	2.12 ± 0.02	2 ± 1	0.14 ± 0.01	3.15 ± 0.16	5215 ± 415
SL10-02	UIC3280	31/40	100-150	2.44 ± 0.13	22 ± 3	2.1 ± 0.1	7.1 ± 0.1	2.07 ± 0.02	5 ± 2	0.19 ± 0.02	3.05 ± 0.16	790 ± 60
SL10-03	UIC2803	29/30	63-100	56.49 ± 1.85	18 ± 2	2.9 ± 0.1	9.0 ± 0.1	1.99 ± 0.02	10 ± 3	0.13 ± 0.01	3.18 ± 0.16	17,140 ± 1110
SL10-08	UIC3279	29/30	100-150	67.45 ± 4.55	21 ± 3	2.4 ± 0.1	7.6 ± 0.1	2.13 ± 0.02	5 ± 2	0.16 ± 0.02	3.16 ± 0.16	21,315 ± 1900
SL10-09	UIC2804	29/30	63-100	29.52 ± 1.47	19 ± 2	3.0 ± 0.1	8.4 ± 0.1	2.10 ± 0.03	5 ± 2	0.15 ± 0.01	3.46 ± 0.18	8510 ± 645
SL10-11	UIC2806	30/35	63-100	5.09 ± 0.25	21 ± 3	2.5 ± 0.1	8.8 ± 0.1	2.21 ± 0.03	5 ± 2	0.17 ± 0.01	3.50 ± 0.18	1440 ± 110
SL10-12	UIC2801	27/30	63-100	0.68 ± 0.03	42 ± 6	3.1 ± 0.1	8.4 ± 0.1	2.16 ± 0.03	5 ± 2	0.18 ± 0.02	3.57 ± 0.18	180 ± 15
SL10-13	UIC3276	28/30	100-150	32.73 ± 1.69	20 ± 3	2.5 ± 0.1	8.5 ± 0.1	2.20 ± 0.02	10 ± 3	0.13 ± 0.01	3.13 ± 0.16	10,440 ± 850
SL10-15	UIC3478	27/30	63-100	19.26 ± 1.10	24 ± 4	2.8 ± 0.1	9.1 ± 0.1	2.12 ± 0.02	5 ± 2	0.17 ± 0.02	3.50 ± 0.18	5490 ± 440
SL10-24	UIC3273	37/40	150-250	31.94 ± 1.61	23 ± 3	2.6 ± 0.1	8.5 ± 0.1	2.20 ± 0.02	10 ± 3	0.12 ± 0.01	3.09 ± 0.16	10,315 ± 830
SL10-26	UIC3479	28/30	63-100	33.75 ± 1.94	24 ± 3	2.6 ± 0.1	9.1 ± 0.1	2.13 ± 0.02	5 ± 2	0.15 ± 0.02	3.44 ± 0.17	9785 ± 795
SL10-28	UIC2802	25/30	63-100	6.66 ± 0.30	22 ± 3	2.7 ± 0.1	8.4 ± 0.1	2.16 ± 0.03	5 ± 2	0.18 ± 0.02	3.48 ± 0.18	1905 ± 140
SL10-30	UIC2805	25/30	63-100	0.23 ± 0.01	50 ± 6	2.0 ± 0.1	7.4 ± 0.1	2.30 ± 0.02	5 ± 2	0.21 ± 0.02	3.02 ± 0.15	70 ± 10

[a] Equivalent dose analyzed under blue-light excitation (470 ± 20 nm) by single aliquot regeneration protocols (Murray and Wintle, 2003; Wintle and Murray, 2006).

[b] Values reflect precision beyond instrumental errors; values of ≤20% (at 2 sigma errors) indicate low dispersion in equivalent dose values with an log-normal unimodal distribution. Overdispersion values of >30% indicates dispersion beyond a single log normal distribution, with possible mixture of grains of various ages; for these analysis the minimum age model was used to calculate the equivalent dose (Galbraith and Roberts, 2012).

[c] U, Th and K_2O content analyzed by inductively coupled plasma-mass spectrometry analyzed by Activation Laboratory LTD, Ontario, Canada.

[d] From Prescott and Hutton (1994).

[f] Ages calculated using the central age model with overdispersion values of ≤20% (at 2 sigma errors) or the minimum age model with overdispersion values of >35% of which weights for the youngest equivalent dose population (Galbraith and Roberts, 2012). All errors are at 1 sigma and ages calculated from the reference year AD 2000.

cut A, Road cut B, Miguel, Esteban, Alfo and Tejon (Fig. 4). These sections are located in different geologic–geomorphic settings of the Mercedes Basin. The Mercedes is one of a series of NNW to SSE rift basins, subparallel to the Pampean Ranges, developed during the Cretaceous and with a sedimentary thickness between 3500 and 4000 m (Yrigoyen et al., 1989; Rossello and Mozetic, 1999). The geometry and stratigraphy of the Mercedes Basin are not completely known (Kostadinoff and Gregori, 2004). It is inferred that this basin remained a foreland depocenter during the Cenozoic Andean Orogeny (Mpodozis and Ramos, 1990), with continental sedimentation through the Tertiary and Quaternary (Costa et al., 2005).

The Esteban and Tejon sections are located on the northern margin of the Mercedes Basin where the crystalline basement is often near the surface (Fig. 1). The Esteban section is at ~570 m altitude in the midst of a southward <1° sloping surface with minimal drainage development, though new rivers have formed in the past decade (Contreras et al., 2013). Tejon section is lower at ~500 m on the same regional slope. The Quinto River overlook, Road cut A and Road cut B sections are situated above the alluvial plain of the Quinto River (Fig. 1), which coincides with a namesake structural lineament (Criado Roque et al., 1981). These sections are adjacent to this river, on a high upland surface at ~430 m asl, that can be traced on either side of the Quinto River and from which the river has degraded by at least 17 m. The eolian sediments at the Quinto River site cover fluvial deposits of possible early Pleistocene or Pliocene age (cf. Costa et al., 2005), which indicates ample accommodation space for this locality, compared with the Esteban and Tejon sections. In contrast, the Alfo section is also on the southern side of the Quinto River but on a higher surface at ~474 m (Fig. 1). The Miguel section is near one depocenter of the Mercedes Basin and is associated at the surface with large complex dunes, with

~0.5 km long, parabolic-like forms, superimposed eolian bedforms (Tripaldi and Forman, 2007) and, in places, more recent (ca. 20th century) small blowout to parabolic dunes (Tripaldi et al., 2013). The Miguel section is at a recent blowout inset into an older, larger blowout area, which now hosts a lake. Hand augering at the base of the Miguel section indicates that eolian sand continues for another 13 m. Despite the different geologic–geomorphic settings and the dissimilar stratigraphic accommodation space all studied sections show 3 to 6 m thick eolian succession of Holocene age.

4.2. Eolian stratigraphic record

4.2.1. Esteban section (33° 32.069′ S; 65° 19.876′ W, 572 m asl)

This 9-m thick section (Figs. 4a and 5a) was exposed in AD 2008 by incision of a newly formed river, north of Villa Mercedes (Contreras et al., 2013). The lowest unit 1 is a dark brown (7.5YR 3.5/4), massive sandy silt with common calcareous nodules, rhizo-concretions (2–5 cm long) and some burrow casts. Above is unit 2 composed of 4.7-m thick, dark yellowish brown (10YR 4.5/4), massive, moderately to poorly sorted, silty sand (Appendix 1). Burrow casts are common in the top of this unit where a 15 cm thick weak, buried A horizon is present. This A horizon is buried by a 10 cm layer of tephra, partially mixed or interlayered with epiclastic sediment (unit 3). The tephra is pale to very pale brown (10YR 6/3–10YR 7/3), massive, or with diffuse millimeter to centimeter-scale horizontal laminations. Capping the tephra is a brown (10YR 4.5/3), 65-cm thick bed of massive to faintly horizontally laminated, moderately sorted silty sand (Fig. 4a).

Quartz grains from the basal 10 cm of unit 2 yielded an OSL age of 10,315 ± 830 yr (UIC3273, Table 1); with higher samples that returned OSL ages of 9785 ± 795 yr (UIC3479) and 1905 ± 140 yr (UIC2802),
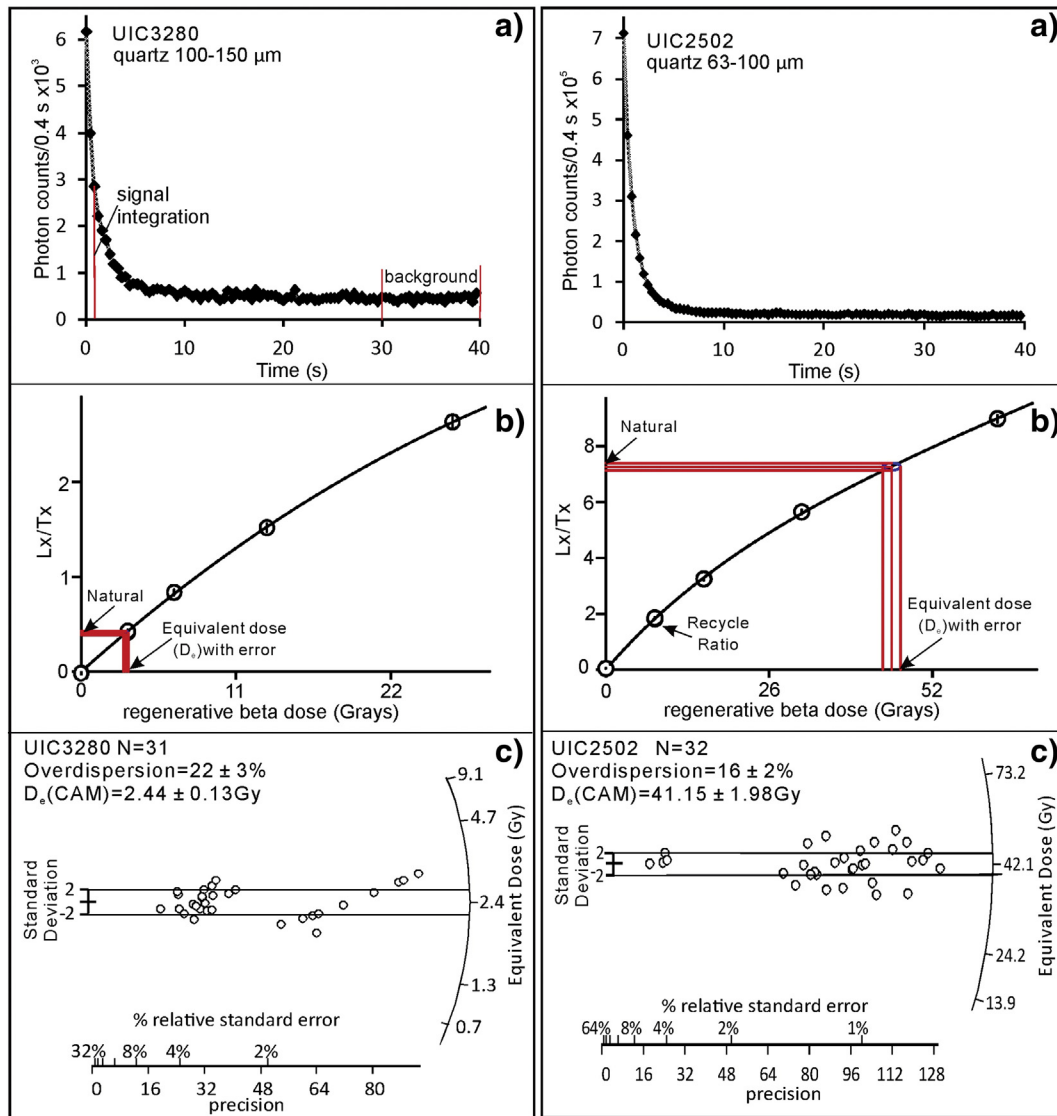
Fig. 3. Optically stimulated luminescence data for quartz grains (samples UIC3280 and UIC2502) from eolian sand sheet deposits. (a) Representative shine down curves of natural luminescence; (b) Regenerative growth curve, showing errors; (c) Radial plots showing statistics for equivalent dose determinations. Mean equivalent dose determined by the central age model (CAM) of Galbraith and Roberts (2012) because of low overdispersion values ≤20% (at two sigma).

respectively. Quartz grains from the base of unit 1 yielded an OSL age of 70 ± 10 yr (UIC2805). This surface eolian sand deposited ca. 70 years old immediately overlies the tephra layer and is consistent with widespread dispersal of ash in central Argentina during the Quizapú volcanic eruption (Chilean Andes) on April, 10 to 11, 1932 (Hildreth and Drake, 1992). The surface soil is weak with a <4 cm thick incipient A horizon.

4.2.2. Miguel section (33° 58.341′ S; 65° 35.298′ W, 497 m asl)

This section is exposed in an east-facing blowout dune "wall" which is composed of ~7 m of eolian fine sand with depositional units differentiated by two paleosols (Fig. 4b). The lowest unit (1) is a yellowish brown (10YR 4.5/3), moderately to well sorted, fine sand with millimeter-scale horizontal lamination. The upper 55 cm of unit 1 is a pedogenically-altered, dark yellowish-brown (10YR 3.5/4), mostly massive fine sand with Machette's (1985) stage 1 to 2 carbonate filaments (BCkb horizon). Unit 2 is a moderately to well sorted fine sand with 10 to 15 cm thick intervals of millimeter-scale horizontal bedding alternating with massive levels. Some beds are laterally discontinuous, have diffuse transitions, and show cm-scale undulatory contacts. The upper contact of unit 2 is demarcated by a weak buried soil (CBwb) that shows noticeable rubification (10YR 3/6), weak blocky structure, and

small root casts. This buried soil has been truncated by emplacement of unit 3, a very well sorted, fine sand. Unit 3 is laterally discontinuous and the buried soil is "welded" to the surface soil (cf. Ruhe and Olson, 1980). Quartz grains from bedded strata in unit 1 yielded OSL ages of 17,140 ± 1110 yr (UIC2803) and 18,130 ± 1300 yr (UIC2345). A sequence of five OSL ages was returned for unit 2 ranging from ca. 11,500 to 800 yr (Table 1, Fig. 4).

4.2.3. Tejon section (33° 40.363′ S; 65° 22.950′ W, 503 m asl)

At this site two distinct eolian depositional units are identified by a bounding paleosol (Fig. 4c). The basal unit 1 is a mostly dark yellowish-brown (10YR 4.5/4), massive, moderately sorted fine silty sand. The top of this unit is differentiated by a weak buried soil with a 3 to 5 cm thick, dark grayish brown (10YR 3.5/2) Ab horizon. The top of this buried soil is scoured with cm-scale relief and intraclasts of Ab horizon material are common in the lower 5 cm of overlying unit 2. Unit 2 is moderately well sorted, silty sand with mm-scale horizontal laminations in the lower 50 cm and massive sand above the present surface. There is an incipient and discontinuous Ab within the laminated sand distinguished by abundant dark brown (10YR 3/3) mottles and cm-scale burrow casts (Fig. 4c). The surface soil is weak with a 1 to
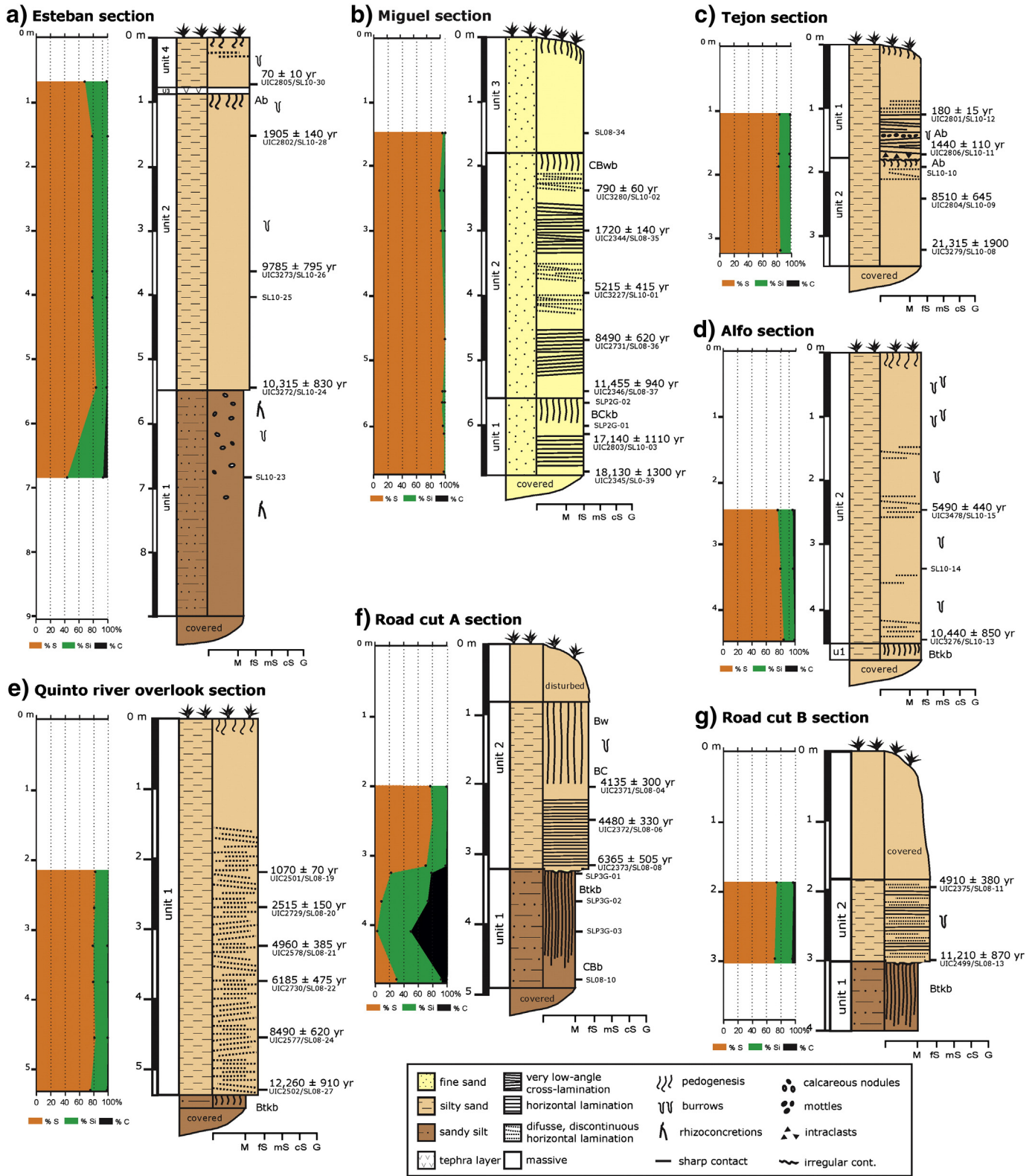
Fig. 4. Stratigraphic sections (a–g) in San Luis paleodune field showing bedding characteristics, buried soils, OSL ages and granulometry. To the left of the sections there is the ratio among sand (S), silt (Si) and clay (C).

3 cm thick A horizon. Quartz grains from unit 1, at 3.2 m and 2.4 m below the present surface, returned OSL ages of 21,315 ± 1900 yr (UIC3279) and 8510 ± 645 yr (UIC2804), respectively (Fig. 4c, Table 1). In turn, quartz grains from unit 2 yielded optical ages of 1440 ± 110 yr (UIC2806) and 180 ± 15 yr (UIC2801).

4.2.4. Alfo section (33° 47.400′ S; 65° 22.713′ W, 474 m asl)

This section is in a sand quarry that exposes up to 5 m of mostly massive, dark yellowish-brown (10YR 4/4) moderately sorted, silty sand (Appendix 1), overlying a well developed paleosol with argillans and Machette's (1985) stage 2 carbonate morphologies (Btkb) (Fig. 4d).

Unit 2 appears to be extensively burrowed with observed 5 to 10 cm long bed remnants; OSL samples were taken from these levels. There is an increase in small carbonate-rich pebbles in the basal 10 cm of unit 2. An OSL age of 10,440 ± 850 yr (UIC3276) was obtained from quartz grain from the base of the succession, 6 cm above the top of the paleosol, whereas a higher sample yielded an OSL age of 5490 ± 440 yr (UIC3478) (Fig. 4d, Table 1).

4.2.5. Quinto river overlook (33° 50.333′ S; 65° 14.669′ W, 432 m asl)

This section exposes ~5.5 m of very fine sand (unit 1), overlying a brown, dense paleosol (Btkb horizon). The lower ~3.2 m of unit 1 show a diffuse, millimeter-scale, horizontal to very low angle (<5°) cross-lamination, whereas the upper 2 m is massive and altered pedogenically (Fig. 4e). The granulometry of this deposit is homogeneous composed of moderately sorted, silty sand (Table 1). OSL ages on quartz grains from bedded intervals for this succession range from ca. 12.3 ka to 1.1 ka (Fig. 4e, Table 1).

4.2.6. Road cut A (33° 50.353′ S; 65° 14.619′ W, 434 m asl)

This section is similar to the Quinto River overlook section with >3 m thick, silty sand and beneath a well developed paleosol (Fig. 4f). The basal paleosol (Btkb) is developed throughout unit 1 and is a reddish brown (5YR 4/5) silty clay with abundant argillans and siltans, Machette's (1985) stage 2 carbonate filaments, and strong medium sub-angular blocky structure. Unit 3 sits unconformably over unit 2 paleosol and is a dark yellowish-brown (10YR 4.5/4), moderately sorted, silty sand, with the lower 1.2 m exhibiting millimeter-scale horizontal laminations (Fig. 5d). Quartz grains from the base of unit 3 returned an OSL age of 6365 ± 505 yr (UIC2373) and two overlying samples yielded OSL ages of 4480 ± 330 yr (UIC2372) and 4135 ± 300 yr (UIC2371) (Fig. 4b, Table 1).

4.2.7. Road cut B (33° 50.353′ S; 65° 14.584′ W, 434 m asl)

This site has a similar stratigraphy to Road cut A, which is 50 m to the west with a well developed paleosol (Btkb) capped by moderately sorted, very fine silty sand (Fig. 4g). Only the basal 1.3 m of this silty sand was exposed, but exhibited millimeter-scale horizontal laminations and these beds were sampled to determine the initiation of eolian sedimentation. The laminated sand of unit 2 is chronologically constrained by two OSL ages yielding, at the base, 11,210 ± 870 yr (UIC2499) and 4910 ± 380 yr (UIC2375) above (Table 1).

4.3. Particle size

There are distinct granulometric differences between sections, particularly within the upper units composed of sand. These sediments present unimodal and symmetric to asymmetric particle size distributions (Appendix 1). Sediments within ~60 cm of paleosols are often poorly to very poorly sorted reflecting higher amounts of silt (>55%) and clay (24 to 52%; Appendix 1) reflecting either the translocation of fine particles or eolian reworking of buried soils This finer texture is particularly prominent for sediment from the Quinto River sections where there is an underlying silty-clay paleosol (Fig. 6b). This granulometry indicates that emplacement of the eolian sands was initially erosive to the underlying paleosol, possibly with stripping of an A horizon and associated vegetation; the presence of intraclasts and pedogenic carbonate small pebbles (Tejon and Alfo sections, Fig. 4) supports this interpretation. Sediment from the Miguel section is a moderately to well sorted, fine sand with less than 5% silt and traces of clay, similar to San Luis dune deposits (Fig. 6). In contrast, the remaining sections are composed of moderately to poorly sorted, silty sand with up to 7% of clay (Appendix 1, Fig. 6). These particle size distributions (Fig. 6) are consistent with previously reported sand sheet deposits (Pye and Tsoar, 2009: 75; Lea, 1990), which show poorly sorted sediments, with variable
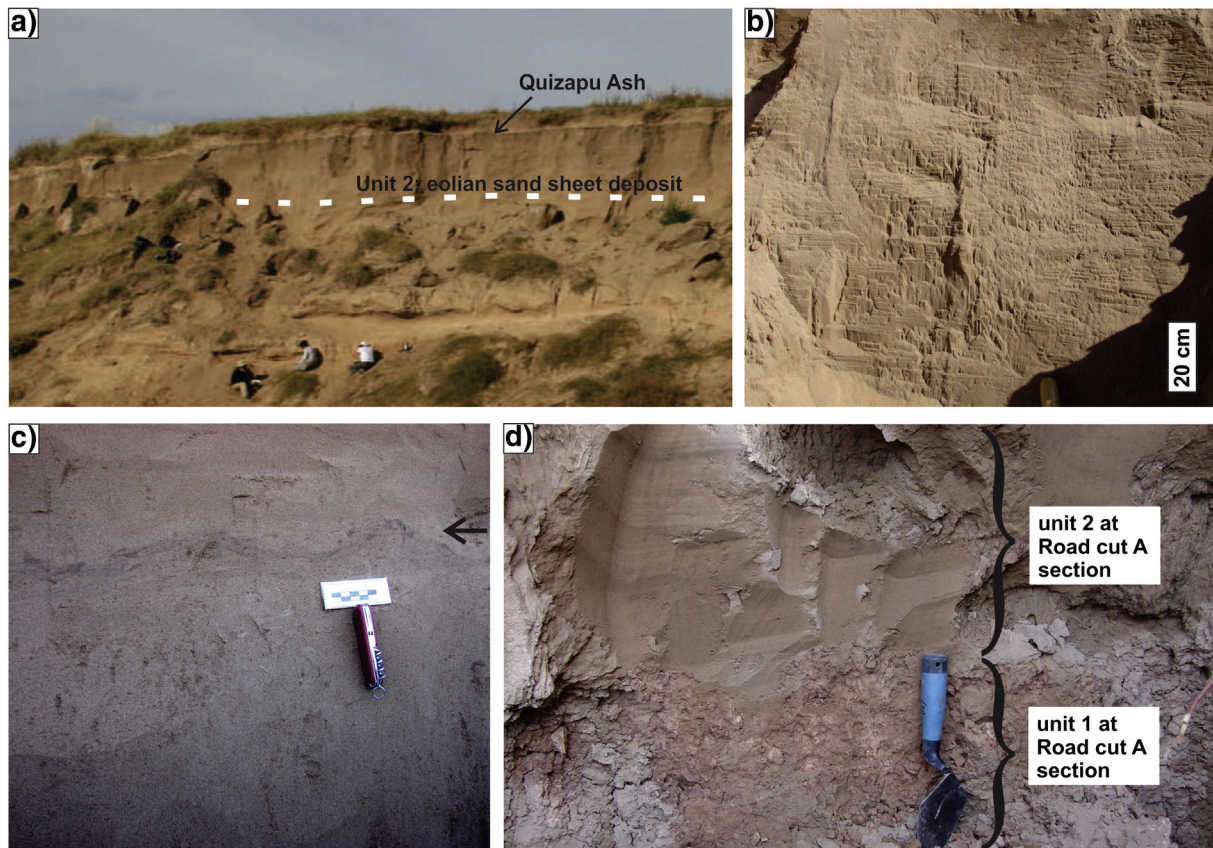

Fig. 5. Photographs of field sites: (a) Esteban section, note light bed near top of section is the 1932 Quizapú Ash; (b) undulatory bedding and incipient buried soil (arrowed) at the Tejon section, scale is 5 cm; (c) horizontal laminated fine sand at the Miguel Site in unit 2; (d) contact between Holocene sand sheet deposit and underlying buried soil at Road cut A section.

mean particle sizes and appreciable amounts of silt (>5%). Sediment in the Miguel section is significantly coarser and the particle size distribution is similar to dune sands (Pye and Tsoar, 2009: 75; Lea, 1990). The granulometry of San Luis eolian sediments resembles sand sheet deposits from northwestern Argentina and is significantly coarser than Pampean loess (Fig. 6).

4.4. Petrography and geochemistry

The mineralogy of the Holocene eolian sand is relatively homogenous (Fig. 7). These deposits are dominated by lithic fragments (34–53% of whole sand) derived mainly from volcanic rocks (Fig. 7b) and with appreciable abundance of quartz (18–33%) and plagioclase (10–18%) and lesser quantities of K-feldspars (~10%) (Appendix 2). The amount of volcanic glass is variable (9–20%) but is present in most sediment. In particular, glass shards and pumices show clay rims and they are sub-rounded indicating reworking or weathering. The Holocene sands are petrographically similar to older Pleistocene eolian sands from the San Luis paleodune field (Tripaldi et al., 2010), especially in the dominance of volcanic fragments in the lithic component (Fig. 7b) and the variable and high amount of glass shard and pumice (Fig. 7c). This data indicate that Holocene sands are more likely derived from reworking of late Pleistocene eolian deposits (Tripaldi and Forman, 2007).

Major, minor and some rare earth elements were determined by ICP-MS on 21 samples from the Holocene sand sheet and on 7 sediments from underlying late Pleistocene deposits (Appendix 3). SiO_2 and K_2O percentages for Holocene sediments are highly uniform with mean values (1 sigma errors) of $67.13 \pm 1.23\%$ and $2.59 \pm 0.09\%$ (Fig. 7d). Rare earth elements (Th/Sc versus Zr/Sc) also show similar uniformity (Fig. 7e). There is no statistical difference (1 sigma errors) between Holocene and late Pleistocene sediment in respect to major, minor and rare earth elements (Appendix 3), consistent with the petrographic analysis that late Pleistocene sediment is a likely source for the Holocene sand sheet.

5. Discussion

5.1. Eolian sand sheet deposits of San Luis paleodune field

The observed sedimentary structures of centimeter-to-millimeter-scale, horizontal to subhorizontal laminations that alternate with massive levels or diffuse bedding (Figs. 4 and 5) reflect depositional process in a sand sheet environment where sedimentation occurs by ripple migration and associated with unrippled, flat or undulatory surfaces (Fryberger et al., 1979; Pye and Tsoar, 2009). Massive beds dominated by very fine sand and medium to coarse silt may reflect fine-particle transport by short-term suspension and modified saltation that hampers the development of ripples (Lea, 1990). Such massive sediments occur at the Esteban site, which contain >17% silt and OSL ages that indicate rapid sedimentation ca. 10.3 to 9.8 ka in the lower 2.3 m of unit 3 (Fig. 5). Alternatively, massive levels may occur with post-depositional bioturbation, as observed at the Alfo site. The granulometry and sedimentary structures of the eolian sand sequences are similar to sediments that accumulate in an eolian sand sheet environment (Fryberger et al., 1979). The granulometry of San Luis Holocene sands is a fine to very fine sand (>69%) to a silty sand, with variable amounts of silt (<20%) (Appendix 1). Sand sheet deposits often exhibit higher percentages of silt, compared to dune facies (Pye and Tsoar, 2009, p. 245–247). A fraction of the fine-very fine sand and silt may correspond to the presence of phytoliths considering the inferred grassland setting of the sand sheet.

The petrography and sediment geochemistry indicate that the dominant source for sand sheet deposits is previously deposited late Pleistocene eolian deposits (Fig. 7). Granulometry of these sediments indicates two distinct subfacies for this eolian sand sheet. The

dominance of a moderately to well sorted, fine sand with <4% silt at Miguel section is interpreted as a proximal sand sheet deposit (Fig. 6), with adjacent Pleistocene dune deposits providing an ample sediment supply. In contrast, eolian sediments from near the Quinto River and on upland surfaces (Fig. 1b) are a poorly sorted fine to very fine sands with up to 20% silt (Appendix 1) and reflect distal deposition from a Pleistocene dune sand source (Fig. 6); these deposits are texturally similar to active sand sheets from northwestern Argentina (Tripaldi, 2002).

OSL ages indicate that sand sheet deposition initiated ca. 12.3 to 10.3 ka, about simultaneous to the Younger Dryas chronozone (~12.8–11.6 ka, Björck, 2006) and often buries a well-developed soil formed in late Pleistocene deposits (Figs. 4 and 8e). The sequence of OSL ages at the Quinto River overlook, Esteban, Alfo and the Miguel sites indicate nearly continuous accretion of the sand sheet through the Holocene, which is supported by the presence of bedding structures with millimeter-to-centimeter scale horizontal to low angle (<5°) beds. Field observations and associated laboratory analyses indicate no discernible buried soils, changes in granulometry, mineralogy or angular unconformities within the sand sheet deposit, which indicates nearly continuous deposition. However, the frequency distribution (n = 28) of OSL ages (Fig. 8) may be a minimum representation of the actual age structure and more OSL ages at these sites and other sites are needed to test this apparent distribution.

5.2. Paleoenvironmental and paleoclimatological implications

The eolian sand sheet deposits occur in diverse geologic settings in the Mercedes Basin from near the depocenter to marginal areas (Kostadinoff and Gregori, 2004). These sediments are also identified in varying geomorphic context including low gradient surfaces with minimal fluvial dissection, to upland surfaces adjacent to the Quinto River, and in a late Pleistocene paleodune field (cf. Tripaldi and Forman, 2007). In all these settings the petrography and geochemistry indicate that the sand is locally derived from preexisting Pleistocene eolian deposits, suggesting decreased vegetation cover and/or increased wind speeds to access the underlying eolian sand (cf. Pye and Tsoar, 2009, p. 127–145). Field-based studies and ecosystem simulations indicated that when vegetation cover (grasses) is reduced below a threshold of ~30% in response to a decrease in effective moisture and other landscape disturbances (e.g. grazing or fire) the underlying sand is sufficiently exposed for eolian entrainment (Mangan et al., 2004; Kuriyama et al., 2005; Pye and Tsoar, 2009, p. 113). This pervasive eolian sand sheet deposit of the San Luis paleodune field spanning much of Holocene is likely associated with a sparse vegetation cover, mostly scattered bushes, similar to the present Monte ecotone, approximately 200 to 250 km to the west (Abraham et al., 2009). Sand sheet deposition with ripple migration is a common process for currently active eolian environments in western and northwestern Argentina (Tripaldi, 2002), where Monte-type vegetation dominates and annual precipitation is ~300 to 70 mm/yr. This inference on the eastward expansion of semi-arid environments between ca. 12 and 1 ka ago is consistent with nearby pollen records (Fig. 8b), which show the dominances of Monte-indicative species spanning the early to late Holocene (D'Antoni, 1983; Markgraf, 1983; Mancini et al., 2005). In turn, a water level record for Mar Chiquita Lake (Fig. 1) indicates low water levels for ca. 14 to 1 ka, with the lowest stands at ca. 14 ka, 8.2 ka, and between 5 and 3 ka (Fig. 8c).

A number of proxy climatic records from western Argentina indicates sustained dry conditions (MAP <450 mm) for much of the Holocene (Fig. 8) and thus, the excessively wet conditions (MAP >700 mm) in the late 20th and 21st centuries are particularly anomalous (cf. Pasquini et al., 2006; Piovano et al., 2009; Agosta and Compagnucci, 2012). The 20th century (1900–1998) mean annual precipitation for Villa Mercedes, San Luis Province, is 552 ± 121 mm (Compagnucci et al., 2002), and during the drought years in the 1930s precipitation decreased by 33 to 62%, which was associated with a
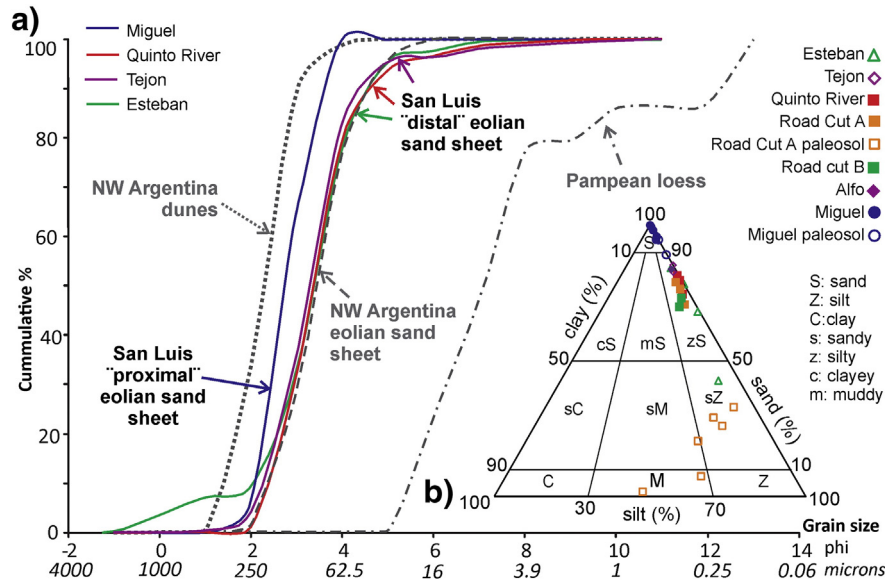
Fig. 6. Cumulative percentage curves for sand sheet deposits in San Luis Province compared with Pampean loess (Teruggi, 1957) and active dunes and sand sheet in northwestern Argentina (Tripaldi, 2002). Granulometry is shown for representative samples from Miguel (SL10-36), Quinto River overlook (SL08-20), Tejon (SL10-10), and Esteban (SL10-28) sections (see Fig. 4). Inset diagram is a ternary plot for particle size for these sediments. Additional information is in Appendix 1.
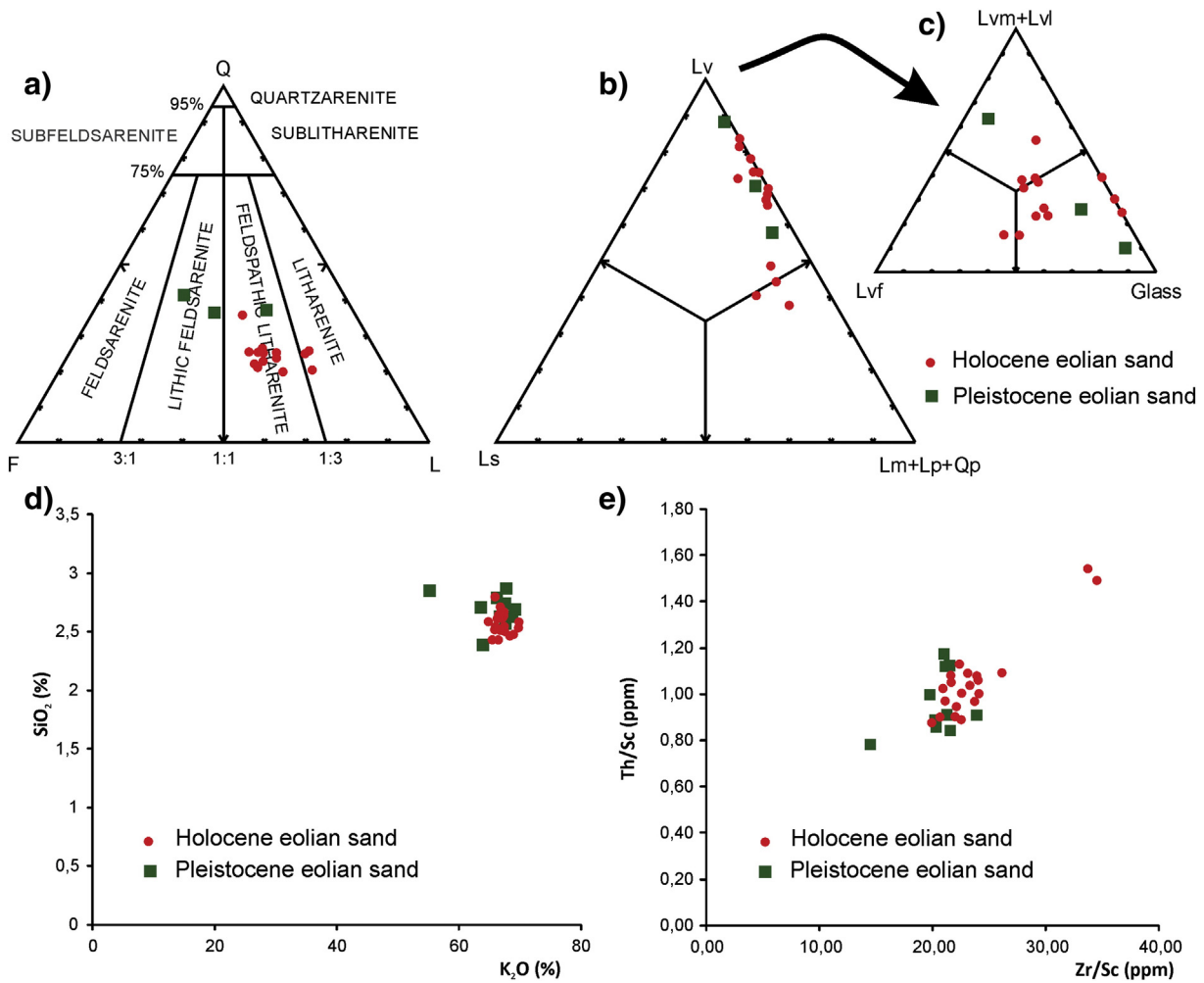

Fig. 7. Petrographic and geochemical data for bulk eolian sediments from the Sand Luis paleodune field showing the Holocene sand grains are similar to older late Pleistocene sands: (a) QFL classification according to Folk et al. (1970); (b) ternary distribution of sedimentary lithic (Ls), volcanic lithic (Lv) and metamorphic and plutonic lithics plus polycrystalline quartz (Lm + Lp + Qp); (c) ternary distribution of glass (glass), felsic (Lvf) and basic (Lvm + Lvl) volcanic fragments; (d) relation between silica (SiO_2) and potassium (K_2O); (e) relation between the ratio of thorium/scandium (Th/Sc) and zirconium/scandium (Zr/Sc). Additional information is in Appendices 2 and 3.

sparse vegetation cover and widespread reactivation of dune systems (Tripaldi et al., 2013). Dry conditions in the western Pampas are coincident with rising and sustained SSTs in the western South Atlantic Ocean (Fig. 8d; Pivel et al., 2013), which implies a weakened gradient between the South Atlantic Anticyclone and the Chaco Low and reduced moisture flux to western Argentina (Compagnucci et al., 2002; Doyle and Barros, 2002; Barros et al., 2008). In contrast, speleothems from Botuverá Cave in southeast Brazil indicate increasing monsoonal precipitation for the past ca. 11 ka (Fig. 8a) consistent with the 20th and 21st centuries' "dipole" climatology, with a wet, coastal southeast Brazil concomitant with a dry western Argentina (Doyle and Barros et al., 2002; Cruz et al., 2009). Increasingly wet conditions for Botuverá Cave are associated with rising summer insolation values through the Holocene (Wang et al., 2006). However, there is one noticeable anomaly at ca. 8.2 ka with a >0.5‰ sharp decrease in speleothem δO^{18} values associated with wetter conditions (Fig. 8a) apparently coincident with 2 °C drop in SSTs in the western South Atlantic Ocean (Fig. 8d), a fall in lake level in Mar Chiquita (Fig. 8c) and more broadly related to sand sheet sedimentation (Fig. 8e). The 8.2 ka event is well documented as the last major meltwater incursion into the North Atlantic Ocean from the retreating Laurentide ice sheet (cf. Barber et al., 1999; Hoffman et al., 2012). This cooling for western subequatorial Atlantic Ocean appears to have initiated earlier at ca. 10 ka, with a peak cooling at 8.2 ka and subsequent quick recovery to warmer SSTs (Fig. 8d). Global climate modeling of the cooling of the equatorial Atlantic Ocean at ca. 8.2 ka indicates a suppressed southward expansion of the South American Monsoon and reduced flux of effective moisture into western Argentina (Morrill et al., 2013), consistent with ensuing sand sheet accretion (Fig. 8e). This drying in the subtropics east of the Andes in South America may be sustained for much of Holocene as indicated by a climate reconstruction at 6 ka based on the ensemble mean output of 17 atmospheric and 11 coupled ocean–atmosphere general circulation models (Zhao and Harrison, 2012). Sustained sand sheet deposition between 7 and 4 ka (Fig. 8e) is partially coincident with a low water phase in Mar Chiquita between 5 and 3 ka, though this interval lacks age control (Piovano et al., 2009). Pronounced aridity is inferred farther to the west in San Juan Province, where high angle cross-beds of a large longitudinal dune filled a drainage and associated quartz grains yielded OSL ages of ca. 4.2 ka (Tripaldi and Forman, 2007). Dune systems in La Rioja Province also show activation at ca. 2.5 ka, also associated with regional drying (Tripaldi and Forman, 2007). Sand sheet sedimentation appears to cease after ca. 0.8, 0.5, and 0.2 ka ago at Miguel, Quinto River and Tejon sites, respectively, and is consistent with the latest episode of dune migration between 0.6 and 0.4 ka for paleodune systems to the northwest (Tripaldi and Forman, 2007). Wetter conditions appear to prevail post the Medieval Climate Anomaly (ca. AD 1200) (cf. Piovano et al, 2009) with ensuing succession to Espinal vegetation and a wetter climate prior to European settlement (cf. Contreras et al., 2013).

6. Conclusions

Sand sheets deposits are ubiquitous in San Luis Province, western Argentina, and the stratigraphy, sedimentology and OSL ages on quartz grains indicate nearly continuous deposition from ca. 12 to 1 ka ago. Petrography and geochemistry of eolian sediments indicate the source of particles from reworking of older late Pleistocene deposits. Considerably drier conditions (MAP 450–100 mm) are inferred between ca. 12 and 1 ka than the late 20th century (~700 mm) (Agosta and Compagnucci, 2008), with a sparse, Monte-type vegetation cover which increased the availability of particles to accrete this sand sheet. This paleoenvironmental inference is consistent with nearby pollen
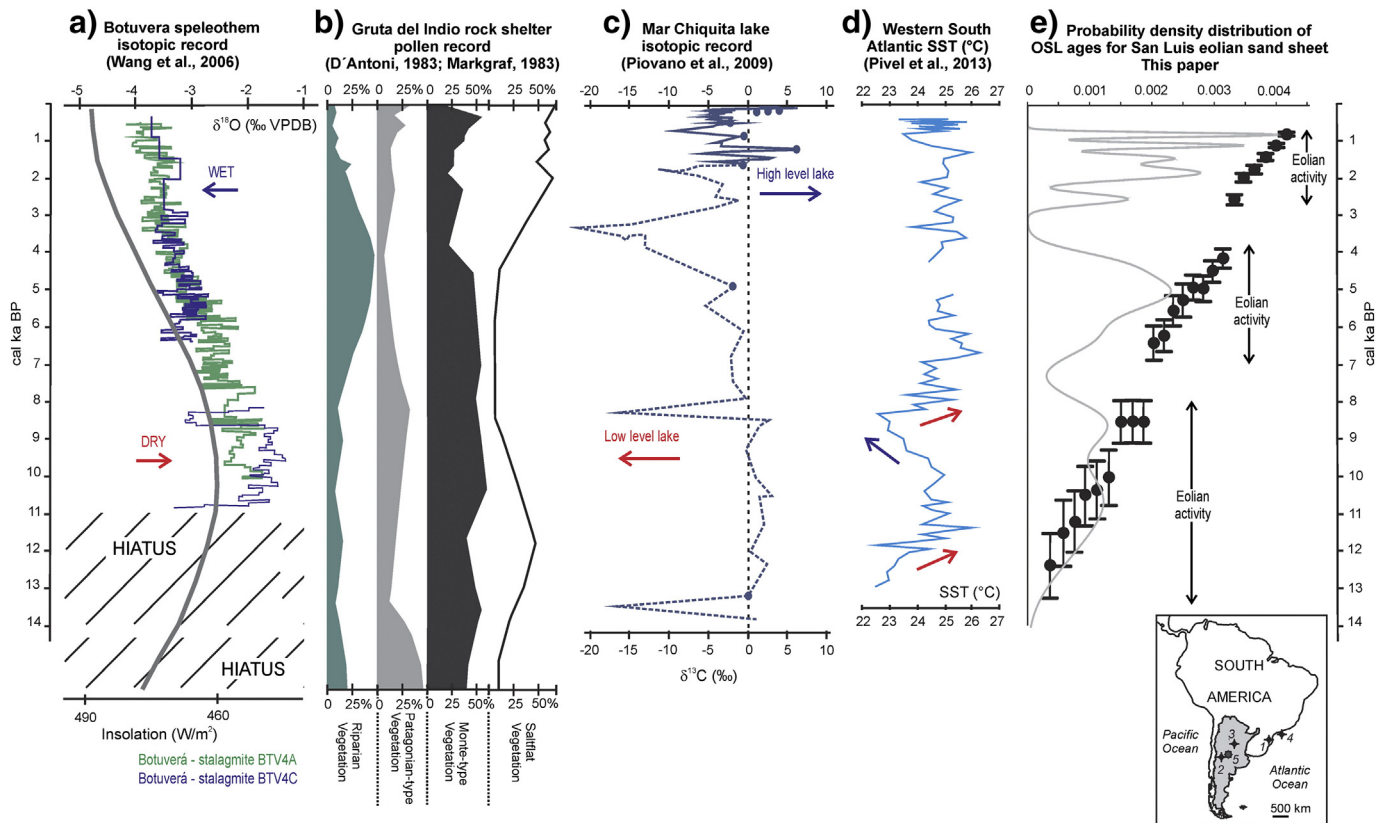
Fig. 8. Comparison among the probability density distribution of OSL ages for San Luis eolian sand sheet deposits (e) with a record of marine core derived SSTs, Brazilian platform (a) (Pivel et al., 2013), a paleo-water level record for Mar Chiquita lake, northern Pampas (b) (modified from Piovano et al., 2009), a pollen record from Gruta del Indio rock shelter, western Argentina (c) (modified from D'Antoni, 1983; Markgraf, 1983) and Botuverá speleothem records, southeastern Brazil (d) (Wang et al., 2006).

records that show an increase in Monte-type vegetation and low water levels for Mar Chiquita Lake in western Argentina during most of the Holocene (Fig. 8; Markgraf, 1983; Mancini et al., 2005; Piovano et al., 2009). A persistent semi-arid environment in western Argentina during the Holocene may reflect sustained warm SSTs in the western subequatorial Atlantic Ocean, which suppresses the pressure gradient between the South Atlantic Anticyclone and Chaco Low and thus the flux of summer moisture to western Argentina. Speleothems from Botuverá Cave in southeastern coastal Brazil yield a contrary but predicted response for the Holocene, with an inferred increase in precipitation, and strengthening of the South American Monsoon. There is a noticeable shift in proxy records at 8.2 ka, associated with equatorial ocean cooling due to the last major meltwater pulse from the Laurentide ice sheet, with a wetter Botuverá Cave record, a pronounce lake level fall in Mar Chiquita. The response of eolian depositional systems in western Argentina during the 8.2 ka event lacks definition because of the paucity ages, but available data indicate that eolian deposition ensued from ca. 9 to 8 ka, with an apparent hiatus in ages ca. 8 to 7 ka with wetter conditions (Fig. 8). This "dipole" climatic response between a dry western Argentina and a wet southeastern Brazil is consistent with 20th and 21st century climatology (Doyle and Barros, 2002) and global climate models (e.g. Morrill et al., 2013). Sand sheet accretion appears to cease in the past ca. 800 to 200 years with wetter conditions and succession to Espinal vegetation prior to European contact.

Supplementary data to this article can be found online at http://dx.doi.org/10.1016/j.palaeo.2014.05.038.

References

Abbott, M.B., Wolfe, B.B., Wolfe, A.P., Seltzer, G.O., Aravena, R., Mark, B.G., Polissar, P.J., Rodbell, D.T., Rowe, H.D., Vuille, M., 2003. Holocene paleohydrology and glacial history of the central Andes using multiproxy lake sediment studies. Palaeogeogr. Palaeoclimatol. Palaeoecol. 194 (1–3), 123–138.

Abraham, E., del Valle, H.F., Roig, F., Torres, L., Ares, J.O., Coronato, R., Godagnone, R., 2009. Overview of the geography of the Monte Desert biome (Argentina). J. Arid Environ. 73, 144–153.

Agosta, E.A., Compagnucci, R.H., 2008. The 1976/77 austral summer climate transition effects on the atmospheric circulation and climate in southern South America. J. Clim. 21, 4365–4383.

Agosta, E.A., Compagnucci, R.H., 2012. Central-West Argentina summer precipitation variability and atmospheric teleconnections. J. Clim. 25, 1657–1677.

Andreoli, R.V., Kayano, M.T., 2004. Multi-scale variability of the sea surface temperature in the Tropical Atlantic. J. Geophys. Res. 109, C05009.

Barber, D.C., Dyke, A., Hillaire-Marcel, C., Jennings, A.E., Andrews, J.T., Kerwin, M.W., Bilodeau, G., McNeely, R., Southon, J., Morehead, M.D., Gagnon, J.M., 1999. Forcing of the cold event of 8,200 years ago by catastrophic drainage of Laurentide lakes. Nature 400 (6742), 344–348.

Barros, V., Doyle, M., González, M., Camilloni, I., Bejarán, R., Caffera, R., 2002. Climate variability over subtropical South America and the South American monsoon: a review. Meteorologica 27, 31–55.

Barros, V.R., Doyle, M.E., Camilloni, I.A., 2008. Precipitation trends in southeastern South America: relationship with ENSO phases and with low-level circulation. Theor. Appl. Climatol. 93, 19–33.

Basu, A., 1985. Influence of climate and relief on compositions of sands released at source areas. In: Zuffa, G.G. (Ed.), Provenance of Arenites. NATO Science Series C, 148, pp. 1–18.

Birkeland, P.W., 1999. Soils and Geomorphology. Oxford University Press, New York.

Björck, S., 2006. Younger Dryas oscillation, global evidence. In: Elias, S.A. (Ed.), Encyclopedia of Quaternary Science, pp. 1985–1993.

Blard, P.H., Sylvestre, F., Tripati, A.K., Claude, C., Causse, C., Coudrain, A., Condom, T., Seidel, J.L., Vimeux, F., Moreau, C., Dumoulin, J.P., Lavé, J., 2011. Lake highstands on the Altiplano (Tropical Andes) contemporaneous with Heinrich 1 and the Younger Dryas: new insights from ^{14}C, U–Th dating and δ^{18}O of carbonates. Quat. Sci. Rev. 30 (27–28), 3973–3989.

Bøtter-Jensen, L., Bulur, E., Duller, G.A.T., Murray, A.S., 2000. Advances in luminescence instrument systems. Radiat. Meas. 32, 523–528.

Cabido, M., Pons, E., Cantero, J.J., Lewis, J.P., Anton, A., 2008. Photosynthetic pathway variation among C4 grasses along a precipitation gradient in Argentina. J. Biogeogr. 35, 131–140.

Cabrera, A.L., 1976. Regiones Fitogeográficas de Argentina. Enciclopedia Argentina de Agricultura y Jardinería. Fascículo I, Tomo II. Editorial ACME, Buenos Aires.

Compagnucci, R.H., Agosta, E.A., Vargas, W.M., 2002. Climatic change and quasi-oscillations in central-west Argentina summer precipitation: main features and coherent behaviour with southern African region. Clim. Dyn. 18 (5), 421–435.

Contreras, S., Santoni, C.S., Jobbágy, E.G., 2013. Abrupt watercourse formation in a semiarid sedimentary landscape of central Argentina: the roles of forest clearing, rainfall variability and seismic activity. Ecohydrology 6 (5), 794–805.

Costa, C., Ortiz Suarez, A., Miró, R., Chiesa, J., Gardini, C., Carugno Durán, A., Ojeda, G., Guerstein, P., Tognelli, G., Morla, P., Strasser, E., Martos, D., 2005. Hoja Geológica 3366-IV, Villa Mercedes, Provincias de Córdoba y San Luis. Boletín, 348. Instituto de Geología y Recursos Minerales, SEGEMAR, Buenos Aires.

Criado Roque, P., Mombrú, C.A., Ramos, V.A., 1981. Estructura e interpretación tectónica. In: Irigoyen, M. (Ed.), Geología y recursos naturales de la provincia de San Luis. Relatorio del 8° Congreso Geológico Argentino. Asociación Geológica Argentina, San Luis, pp. 155–192.

Cruz, F.W., Burns, S.J., Karmann, I., Sharp, W.D., Vuille, M., Cardoso, A.O., Ferrari, J.A., Silva Dias, P., Viana Jr., O., 2005. Insolation-driven changes in atmospheric circulation over the 1962 past 116,000 years in subtropical Brazil. Nature 434, 63–65.

Cruz, F.W., Vuille, M., Burns, S.J., Wang, X., Cheng, H., Werner, M., Edwards, R.L., Karmann, I., Auler, A.S., Nguyen, H., 2009. Orbitally driven east–west antiphasing of South American precipitation. Nat. Geosci. 2, 210–214.

D'Antoni, H., 1983. Polen analysis of Gruta del Indio. Quat. S. Am. Antarct. Peninsula 1, 83–104.

Dickinson, W.R., 1970. Interpreting detrital modes of graywacke and arkose. J. Sediment. Petrol. 40, 695–707.

Doyle, M., Barros, V., 2002. Midsummer low-level circulation in subtropical South America and related precipitation patterns. J. Clim. 15, 3394–3410.

Duller, G.A.T., 2003. Distinguishing quartz and feldspar in single grain luminescence measurements. Radiat. Meas. 37, 161–165.

Fain, J., Soumana, S., Montret, M., Miallier, D., Pilleyre, T., Sanzelle, S., 1999. Luminescence and ESR dating-Beta-dose attenuation for various grain shapes calculated by a Monte-Carlo method. Quat. Sci. Rev. 18, 231–234.

Folk, R.L., Ward, W.C., 1957. Brazos River bar – a study in the significance of grain-size parameters. J. Sediment. Petrol. 27 (1), 3–27.

Folk, R.L., Andrews, P.B., Lewis, D.W., 1970. Detrital sedimentary rock classification and nomenclature for use in New Zealand. N. Z. J. Geol. Geophys. 13, 937–968.

Fryberger, S.G., Ahlbrandt, T.S., Andrews, S.A., 1979. Origin, sedimentary features, and significance of low-angle eolian "sand sheet" deposits, Great Sand Dunes National Monument and Vicinity, Colorado. J. Sediment. Petrol. 49 (3), 733–746.

Galbraith, R.F., Roberts, R.G., 2012. Statistical aspects of equivalent dose and error calculation and display in OSL dating: an overview and some recommendations. Quat. Geochronol. 11, 1–27.

Galbraith, R.F., Roberts, R.G., Laslett, G.M., Yoshida, H., Olley, J.M., 1999. Optical dating of single and multiple grains of quartz from Jinmium rock shelter, northern Australia, part 1, experimental design and statistical models. Archaeometry 41, 339–364.

Garreaud, R., Vuille, M., Compagnucci, R., Marengo, J., 2009. Present-day South American climate. PALAEO3 Special Issue (LOTRED South America), 281, pp. 180–195.

Garzanti, E., Vezzoli, G., Andò, S., Paparella, P., Clift, P.D., 2005. Petrology of Indus River sands: a key to interpret erosion history of the Western Himalayan Syntaxis. Earth Planet. Sci. Lett. 229, 287–302.

Gazzi, P., 1966. Le arenarie del flysch sopracretaceo dell'Appennino modenese; Correlatzioni con il flysch di Monghidoro. Mineral. Petrogr. Acta 12, 69–97.

Gil, A., Zárate, M., Neme, G., 2005. Mid-Holocene paleoenvironments and the arqueological record of southern Mendoza, Argentina. Quat. Int. 132, 81–94.

González, M.A., Maidana, N.I., 1998. Post-Wisconsinian paleoenvironments at Salinas del Bebedero basin, San Luis, Argentina. J. Paleolimnol. 20 (4), 353–368.

Grimm, A.M., 2003. The El Niño impact on the summer monsoon in Brazil: regional processes versus remote influences. J. Clim. 16, 263–280.

Hildreth, W., Drake, R.E., 1992. Volcan Quizapu, Chilean Andes. Bull. Volcanol. 54, 93–125.

Hoffman, J.S., Carlson, A.E., Winsor, K., Klinkhammer, G.P., LeGrande, A.N., Andrews, J.T., Strasser, J.C., 2012. Linking the 8.2 ka event and its freshwater forcing in the Labrador Sea. Geophys. Res. Lett. 39.

Iriondo, M., 1999. Climatic changes in the South American plains: records of a continent-scale oscillation. Quat. Int. 57–58, 93–112.

Iriondo, M., Kröhling, D., 1995. El Sistema Eólico Pampeano. Santa Fe: Comunicaciones del Museo Provincial de Ciencias Naturales Florentino Ameghino, 5(1). Santa Fe, Argentina.

Jenny, B., Valero-Garces, B.L., Villa-Martinez, R., Urrutia, R., Geyh, M., Veit, H., 2002. Early to mid-Holocene aridity in central Chile and the southern Westerlies: the Laguna Aculeo record (34 degrees S). Quat. Res. 58 (2), 160–170.

Kasper-Zubillaga, J.J., Dickinson, W.W., 2001. Discriminating depositional environments of sands from modern source terranes using modal analysis. Sediment. Geol. 143, 149–167.

Kemp, R., Zárate, M., Toms, P., King, M., Sanabria, J., Argüello, G., 2006. Late Quaternary paleosols, stratigraphy and landscape evolution in the Northern Pampa, Argentina. Quat. Res. 66, 119–132.

Kostadinoff, J., Gregori, D.A., 2004. La Cuenca de Mercedes, provincia de San Luis. Rev. Asoc. Geol. Argent. 59 (3), 488–494.

Kuriyama, Y., Mochizuki, N., Nakashima, T., 2005. Influence of vegetation on aeolian sand transport rate from a backshore to a foredune at Hasaki, Japan. Sedimentology 52 (5), 1123–1132.

Labraga, J.C., Villalba, R., 2009. Climate in the Monte Desert: past trends, present conditions, and future projections. J. Arid Environ. 73, 154–163.

Latrubesse, E.M., Stevaux, J.C., Cremon, E.H., May, J.-H., Tatumi, S.H., Hurtado, M.A., Bezada, M., Argollo, J.B., 2012. Late Quaternary megafans, fans and fluvio-aeolian interactions in the Bolivian Chaco, Tropical South America. Palaeogeogr. Palaeoclimatol. Palaeoecol. 356–357, 75–88.

Lea, P.D., 1990. Pleistocene periglacial eolian deposits in southwestern Alaska: sedimentary facies and depositional processes. J. Sediment. Petrol. 60, 582–591.

Liebmann, B., Vera, C.S., Carvalho, L.M.V., Camilloni, I.A., Hoerling, M.P., Allured, D., Barros, V.R., Báez, J., Bidegain, M., 2004. An observed trend in central South American precipitation. J. Clim. 17, 4357–4367.

Machette, M., 1985. Calcic soils of southwestern United States. In: Weide, D.J. (Ed.), Soil and Quaternary Geology of the Southwestern United States. Geological Society of America, Special Paper, 203, pp. 1–21.

Mancini, M.V., Paez, M.M., Prieto, A.R., Stutz, S., Tonello, M., Vilanova, I., 2005. Mid-Holocene climatic variability reconstruction from pollen records (32°–52°S, Argentina). Quat. Int. 132, 47–59.

Mangan, J.M., Overpeck, J.T., Webb, R.S., Wessman, C., Goetz, A.F.H., 2004. Response of Nebraska sand hills natural vegetation to drought, fire, grazing, and plant functional type shifts as simulated by the century model. Clim. Chang. 63, 49–90.

Marengo, J.A., Soares, W., Saulo, C., Nicolini, M., 2004. Climatology of the low-level jet east of the Andes as derived from the NCEP–NCAR reanalyses: characteristics and temporal variability. J. Clim. 17, 2261–2280.

Markgraf, V., 1983. Late and postglacial vegetational and paleoclimatic changes in subantarctic, temperate and arid environments in Argentina. Palynology 7, 43–70.

Markgraf, V., 1989. Palaeoclimates in central and south America since 18,000 BP based on pollen and lake-level records. Quat. Sci. Rev. 8, 1–24.

Mehl, A., Tripaldi, A., Zárate, M.A., 2012. Análisis sedimentológico y cronología del registro cuaternario en el Valle Utracán-Argentino, provincia de La Pampa, Argentina. XIII Reunión Argentina de Sedimentología, Actas. Asociación Argentina de Sedimentología, Salta, pp. 138–139.

Meier, H.A., Nordt, L.C., Forman, S.L., Driese, S.G., 2013. Late Quaternary alluvial history of the middle Owl Creek drainage basin in central Texas: a record of geomorphic response to environmental change. Quat. Int. 306, 24–41.

Mejdahl, V., Christiansen, H.H., 1994. Procedures used for luminescence dating of sediments. Boreas 13, 403–406.

Mendes da Silva, G.A., Ambrizzi, T., 2010. Summertime moisture transport over Southeastern South America and extratropical cyclones behavior during inter-El Niño events. Theor. Appl. Climatol. 101, 303–310.

Morrill, C., LeGrande, A.N., Renssen, H., Bakker, P., Otto-Bliesner, B.L., 2013. Model sensitivity to North Atlantic freshwater forcing at 8.2 ka. Clim. Past 9 (2), 955–968.

Mpodozis, C., Ramos, V., 1990. The Andes of Chile and Argentina. In: Eriksen, G.E., Pinochet, M.T.C., Reinemund, J.A. (Eds.), Geology of the Andes and its relation to hydrocarbon and mineral resources, Circum-Pacific Council for Energy and Mineral Resources. Earth Science Series, 11, pp. 59–90 (Houston).

Murray, A.S., Wintle, A.G., 2003. The single aliquot regenerative dose protocol: potential for improvements in reliability. Radiat. Meas. 37, 377–381.

Olley, J., Caitcheon, G., Murray, A., 1998. The distribution of apparent dose as determined by optically stimulated luminescence in small aliquots of fluvial quartz: implications for dating young sediments. Quat. Sci. Rev. 17, 1033–1040.

Paruelo, J.M., Jobbágy, E.G., Oesterheld, M., Golluscio, R.A., Aguiar, M.R., 2007. The grasslands and steppes of Patagonia and the Rio de la Plata plains. In: Veblen, T., Young, K., Orme, A. (Eds.), The Physical Geography of South America. The Oxford Regional Environments Series. Oxford University Press, pp. 232–248.

Pasquini, A.I., Lecomte, K.L., Piovano, E.L., Depetris, P.J., 2006. Recent rainfall and runoff variability in central Argentina. Quat. Int. 158, 127–139.

Pease, P.P., Tchakerian, V.P., 2003. Geochemistry of sediments from Quaternary sand ramps in the southeastern Mojave Desert, California. Quat. Int. 104 (1), 19–29.

Piovano, E.L., Ariztegui, D., Bernasconi, S.M., Mckenzie, J.A., 2004. The isotopical record of hydrological changes in subtropical South America over the last 230 years. The Holocene 14, 525–535.

Piovano, E.L., Ariztegui, D., Córdoba, F., Cioccale, M., Sylvestre, F., 2009. Hydrological variability in South America below the tropic of capricorn (Pampas and Eastern Patagonia, Argentina) during the last 13.0 ka. In: Vimaux, Ka,F., et al. (Eds.), Past Climate Variability in South America and Surrounding Regions. Developments in Paleoenvironmental Research, 14, pp. 323–351.

Pivel, M.A.G., Santarosa, A.C.A., Toledo, F.A.L., Costa, K.B., 2013. The Holocene onset in the southwestern South Atlantic. Palaeogeogr. Palaeoclimatol. Palaeoecol. 374, 164–172.

Placzek, C., Quade, J., Betancourt, J.L., Patchett, P.J., Rech, J.A., Latorre, C., Matmon, A., Holmgren, C., English, N.B., 2009. Climate in the dry central Andes over geologic, millennial, and interannual timescales. Ann. Mo. Bot. Gard. 96, 386–397.

Potter, P.E., Huh, Y., Edmond, J.M., 2001. Deep-freeze petrology of Lena River sand, Siberia. Geology 29, 999–1002.

Powers, M.C., 1953. A new roundness scale for sedimentary particles. J. Sediment. Petrol. 23 (2), 117–119.

Prescott, J.R., Hutton, J.T., 1994. Cosmic ray contributions to dose rates for luminescence and ESR dating: large depths and long-term time variations. Radiat. Meas. 23, 497–500.

Pye, K., Tsoar, H., 2009. Aeolian Sand and Sand Dunes, Second edition. Springer, Berlin (476 pp.).

Rossello, E.A., Mozetic, M.E., 1999. Caracterización estructural y significado geotectónico de depocentros cretácicos continentales del centro–oeste argentino. 5° Simposio do Cretacico do Brasil & 1° Simposio sobre el Cretácico de América del Sur, Serra Negra. Universidade Estadual Paulista, Brazil, pp. 107–113.

Ruhe, R.V., Olson, C.G., 1980. Soil welding. Soil Sci. 130, 132–139.

Salio, P., Nicolini, M., Saulo, C., 2002. Chaco low-level jet events characterization during the austral summer season. J. Geophys. Res. 107 (D24), 4816.

Sandweiss, D.H., Maasch, K.A., Anderson, D.G., 1999. Transitions in the Mid-Holocene. Science 83 (5401), 499–500.

Seager, R., Naik, N., Baethgen, W., Robertson, A., Kushnir, Y., Nakamura, J., Jurburg, S., 2010. Tropical oceanic causes of interannual to multidecadal precipitation variability in Southeast South America over the past century. J. Clim. 23, 5517–5539.

Silva, V.B.S., Kousky, V.E., 2012. The South American Monsoon System: climatology and variability. In: Wang, S., Gillies, R.R. (Eds.), Modern Climatology. InTech. http://dx.doi.org/10.5772/2014 (398 pp.).

Singhvi, A.K., Porat, N., 2008. Impact of luminescence dating on geomorphological and palaeoclimate research in drylands. Boreas 37 (4), 536–558.

Tchilinguirian, P., Morales, M.R., 2013. Mid-Holocene paleoenvironments in Northwestern Argentina: main patterns and discrepancies. Quat. Int. 307, 14–23.

Teruggi, M.E., 1957. The nature and origin of Argentine loess. J. Sediment. Petrol. 27, 322–332.

Toledo, F.A.L., Costa, K.B., Pivel, M.A.G., 2007. Salinity changes in the western tropical South Atlantic during the last 30 kyr. Glob. Planet. Chang. 57, 383–395.

Tripaldi, A., 2002. Análisis sedimentológico de depósitos eólicos de valles intermontanos, su aplicación al estudio de secuencias terciarias del noroeste argentino. Ph.D Thesis Universidad de Buenos Aires, Argentina.

Tripaldi, A., Forman, S.L., 2007. Geomorphology and chronology of Late Quaternary dune fields of western Argentina. Palaeogeogr. Palaeoclimatol. Palaeoecol. 251, 300–320.

Tripaldi, A., Ciccioli, P.L., Alonso, M.S., Forman, S.L., 2010. Petrography and geochemistry of late Quaternary dune fields of western Argentina: provenance of aeolian materials in southern South America. Aeolian Res. 2 (1), 33–48.

Tripaldi, A., Zárate, M.A., Forman, S.L., Badger, T., Doyle, M., Ciccioli, P.L., 2013. Geological evidence for a drought episode in the western Pampas (Argentina, South America) during the early–mid 20th century. The Holocene 23 (12), 1729–1744.

Viglizzo, E.F., Frank, F.C., Carreño, L.V., Jobbágy, E.G., Pereyra, H., Clatt, J., Pincén, D., Riccard, M.F., 2010. Ecological and environmental footprint of 50 years of agricultural expansion in Argentina. Glob. Chang. Biol. 17 (2), 959–973.

Villagrán, C., Varela, J., 1990. Palynological evidence for increased aridity on the Central Chilean during the Holocene. Quat. Res. 34, 198–207.

Wang, M., Paegle, J., 1996. Impact of analysis uncertainty upon regional atmospheric moisture flux. J. Geophys. Res. 101 (D3), 7291–7303.

Wang, X., Auler, A.S., Edwards, R.L., Cheng, H., Ito, E., Solheid, M., 2006. Interhemispheric anti-phasing of rainfall during the last glacial period. Quat. Sci. Rev. 25, 3391–3403.

Wintle, A.G., Murray, A.S., 2006. A review of quartz optically stimulated luminescence characteristics and their relevance in single-aliquot regeneration dating protocols. Radiat. Meas. 41, 369–391.

Wright, D., Forman, S.L., Waters, M., Ravesloot, J., 2011. Holocene eolian activity as a proxy for broad-scale landscape change on the Gila River Indian Community, Arizona. Quat. Res. 76 (1), 10–21.

Yrigoyen, M., Ortiz, A., Manoni, R., 1989. Cuencas sedimentarias de San Luis. In: Chebi, G.A., Spalletti, L.A. (Eds.), Cuencas Sedimentarias Argentinas. Serie de Correlación Geológica, 6, pp. 203–220 (Tucumán).

Zárate, M., 2003. Loess of southern South America. Quat. Sci. Rev. 22, 1987–2006.

Zárate, M., Tripaldi, A., 2012. The aeolian system of central Argentina. J. Aeol. Res. 3, 401–417.

Zárate, M., Neme, G., Gil, A., 2005. Mid-Holocene paleoenvironments and human occupation in southern South America. Quat. Int. 132, 1–3.

Zech, W., Zech, M., Zech, R., Peinemann, N., Morras, H., Moretti, L., Ogle, N., Kalim, R., Fuchs, M., Schad, P., Glaser, B., 2009. Late Quaternary palaeosol records from subtropical (38° S) to tropical (16° S) South America and palaeoclimatic implications. Quat. Int. 196, 107–120.

Zhao, Y., Harrison, S.P., 2012. Mid-Holocene monsoons: a multi-model analysis of the interhemispheric differences in the response to orbital forcing and ocean feedbacks. Clim. Dyn. 39, 1457–1487.